Identification of a selective and direct NLRP3 inhibitor to treat inflammatory disorders

Hua Jiang,[1,2,3]* Hongbin He,[1]* Yun Chen,[4]* Wei Huang,[4] Jinbo Cheng,[1] Jin Ye,[1] Aoli Wang,[1,6] Jinhui Tao,[5] Chao Wang,[1] Qingsong Liu,[1,6] Tengchuan Jin,[1] Wei Jiang,[1,3] Xianming Deng,[4] and Rongbin Zhou[1,2,3]

[1]Institute of Immunology and the CAS Key Laboratory of Innate Immunity and Chronic Disease, CAS Center for Excellence in Molecular Cell Sciences, School of Life Sciences and Medical Center, [2]Innovation Center for Cell Signaling Network, and [3]Hefei National Laboratory for Physical Sciences at Microscale, University of Science and Technology of China, Hefei, China
[4]State Key Laboratory of Cellular Stress Biology, Innovation Center for Cell Signaling Network, School of Life Sciences, Xiamen University, Xiamen, Fujian, China
[5]Department of Rheumatology and Immunology, Anhui Provincial Hospital Affiliated to Anhui Medical University, Hefei, Anhui, China
[6]High Magnetic Field Laboratory, Chinese Academy of Sciences, Hefei, Anhui, China

The NLRP3 inflammasome has been implicated in the pathogenesis of a wide variety of human diseases. A few compounds have been developed to inhibit NLRP3 inflammasome activation, but compounds directly and specifically targeting NLRP3 are still not available, so it is unclear whether NLRP3 itself can be targeted to prevent or treat diseases. Here we show that the compound CY-09 specifically blocks NLRP3 inflammasome activation. CY-09 directly binds to the ATP-binding motif of NLRP3 NACHT domain and inhibits NLRP3 ATPase activity, resulting in the suppression of NLRP3 inflammasome assembly and activation. Importantly, treatment with CY-09 shows remarkable therapeutic effects on mouse models of cryopyrin-associated autoinflammatory syndrome (CAPS) and type 2 diabetes. Furthermore, CY-09 is active ex vivo for monocytes from healthy individuals or synovial fluid cells from patients with gout. Thus, our results provide a selective and direct small-molecule inhibitor for NLRP3 and indicate that NLRP3 can be targeted in vivo to combat NLRP3-driven diseases.

INTRODUCTION

The inflammasomes are protein complexes formed by innate immune sensors, including NOD-like receptor (NLR) family members NLRP1, NLRP3, and NLRC4, as well as other non-NLR receptors, such as AIM2 and IFI16 (Martinon et al., 2009; Davis et al., 2011; Jo et al., 2016). Upon activation, the sensor proteins oligomerize and then recruit adaptor protein ASC, which then binds with caspase-1 to form inflammasomes. The assembly of inflammasome results in the cleavage and activation of caspase-1, which then promotes pyroptosis or the maturation and secretion of several proinflammatory cytokines, such as IL-1β or IL-18 (Chen et al., 2009; Liu and Cao, 2016). In contrast to other sensor proteins, NLRP3 can sense many different factors derived from not only pathogen but also environment or host, so the aberrant activation of the NLRP3 inflammasome has been regarded as an important initiator or promoter in a variety of human complex diseases, including type 2 diabetes (T2D), gout, atherosclerosis, and neurodegenerative diseases (Martinon et al., 2006; Duewell et al., 2010; Masters et al., 2010; Zhou et al., 2010; Wen et al., 2011; Heneka et al., 2012; Lamkanfi and Dixit, 2012; Broderick et al., 2015), suggesting that the NLPR3 inflammasome might be a potential target for the treatment of these diseases.

The current available clinical treatment for NLRP3-related diseases is the agents that target IL-1β, including the recombinant IL-1 receptor antagonist anakinra, the neutralizing IL-1β antibody canakinumab, and the soluble decoy IL-1β receptor rilonacept (Dinarello et al., 2012). This approach has been used in clinic for the treatment of cryopyrin-associated autoinflammatory syndrome (CAPS), which is caused by gain-of-function mutations of NLRP3, and has also been tested in clinical trials for other NLRP3-related diseases (Dinarello et al., 2012; Dinarello and van der Meer, 2013). However, there are some concerns regarding this treatment. First, IL-1β production is not the only biological effect of NLRP3 inflammasome activation; the pyroptosis or other proinflammatory factors, such as IL-18 and HMGB1, might also are involved in the pathogenesis of diseases (Lu et al., 2012; Nowarski et al., 2015). Second, IL-1β is produced not

only by the NLRP3 inflammasome but also by other inflammasomes or in an inflammasome-independent way (Davis et al., 2011; Netea et al., 2015), so inhibition of IL-1β function might have more immunosuppressive effects than inhibition of NLRP3 itself. Thus, the inhibitors for NLRP3 inflammasome might be a better choice than the agents that target IL-1β for the treatment of NLRP3-driven diseases.

Although both the components of NLRP3 inflammasome, including NLRP3, NEK7, ASC, and caspase-1, and the related signaling events, including priming, mitochondrial damage, potassium efflux, and chloride efflux, can be targeted to inhibit NLRP3 inflammasome activation, only directly targeting NLRP3 itself can specifically inhibit the NLRP3 inflammasome. A few NLRP3 inflammasome inhibitors, including sulforaphane, isoliquiritigenin, β–hydroxybutyrate (BHB), flufenamic acid, mefenamic acid, 3,4-methylenedioxy-β-nitrostyrene (MNS), parthenolide, BAY 11-7082, INF39, and MCC950 (Juliana et al., 2010; He et al., 2014; Honda et al., 2014; Youm et al., 2015; Daniels et al., 2016; Greaney et al., 2016; Cocco et al., 2017), have been developed, but there is no evidence showing that these compounds can specifically and directly inhibit NLRP3 itself. Sulforaphane is not specific to NLRP3 inflammasome and also has shown inhibitory activity for AIM2 or NLRC4 inflammasome and NF-κB activation (Heiss et al., 2001; Greaney et al., 2016). Isoliquiritigenin is also a potential inhibitor for the NF-κB signaling pathway (Honda et al., 2012). BHB inhibits NLRP3 inflammasome activation by preventing potassium efflux (Youm et al., 2015). Flufenamic acid and mefenamic acid inhibit NLRP3 inflammasome activation through the suppression of chloride efflux (Daniels et al., 2016). Parthenolide, BAY 11-7082, INF39, and MNS have been reported to directly inhibit NLRP3 ATPase activity, but these inhibitors have unspecific roles (Juliana et al., 2010; He et al., 2014; Cocco et al., 2017). MNS has been known to inhibit the activity of tyrosine kinases, such as Src and Syk (Wang et al., 2006). Parthenolide, BAY 11-7082, and INF39 have broad anti-inflammatory activities and can suppress NF-κB activation (Yip et al., 2004; Strickson et al., 2013; Cocco et al., 2017). MCC950 has shown strong NLRP3 inflammasome inhibitory activity and beneficial effects in several mice models of NLRP3-related diseases, but it does not directly inhibit NLRP3–NLRP3, NLRP3–ASC, or NEK7–NLRP3 interaction (Coll et al., 2015; Dempsey et al., 2017), suggesting that it might target an unknown upstream signaling event of the NLRP3 inflammasome. Thus, compounds directly and specifically targeting NLRP3 itself are still not available.

Here, we identified an NLRP3 inflammasome inhibitor, CY-09, that directly bound to the ATP-binding site of the NLRP3 NACHT domain and inhibited its ATPase, oligomerization, and NLRP3 inflammasome activation. More important, we provide evidence showing that directly targeting NLRP3 itself by CY-09 could inhibit NLRP3 inflammasome activation in vivo and had remarkable therapeutic effects on the mouse models of NLRP3-driven diseases, such as T2D and CAPS.

RESULTS

CY–09 specifically blocks NLRP3 activation in macrophages

To provide a potential approach for the treatment of NLRP3-driven diseases, we screened NLRP3 inhibitors in an in-house bioactive compound library and found CFTR$_{(inh)}$-172 (C172), which is an inhibitor for the cystic fibrosis transmembrane conductance regulator (CFTR) channel (Ma et al., 2002), could inhibit NLRP3 inflammasome activation. C172 treatment blocked nigericin–induced caspase-1 activation and IL-1β secretion in LPS-primed bone marrow–derived macrophages (BMDMs; Fig. 1, A–C). In addition, cytosolic LPS–induced noncanonical NLRP3 activation was also suppressed by C172 (Fig. 1 D). We also examined whether C172 had an impact on LPS-induced priming for inflammasome activation. When BMDMs were stimulated with C172 before or after LPS treatment, C172 had no effect on LPS-induced NLRP3 and pro–IL-1β expression (Fig. 1 E), suggesting that C172 did not affect LPS-induced priming. These results indicate that C172 is a specific inhibitor for NLRP3 activation.

Because C172 is an inhibitor for CFTR (Ma et al., 2002), we then examined whether C172 inhibited NLRP3 activation via blocking CFTR activity. $Cftr^{-/-}$ BMDMs produced comparable IL-1β with WT BMDMs when stimulated with nigericin (Fig. 1 F). Moreover, C172 still could block nigericin–induced IL-1β production (Fig. 1 F). These results indicate that C172 blocks NLRP3 activation in a CFTR–independent manner.

Because the inhibitory effects of C172 on NLRP3 activation do not depend on its CFTR–inhibitory activity, we then evaluated the effects of several C172 analogues without CFTR–inhibitory activity, which were described previously (Sonawane and Verkman, 2008), on NLRP3 activation. We found that an analogue, CY-09 (Fig. 2 A), showed comparable activity for NLRP3 inhibition with C172. CY-09 exhibited a dose-dependent inhibitory effect on monosodium urate (MSU), nigericin, and ATP-induced caspase-1 activation and IL-1β secretion at the doses of 1–10 μM in LPS-primed BMDMs (Fig. 2, B–D). Cytosolic LPS–induced noncanonical NLRP3 activation in BMDMs could also be blocked by CY-09 treatment (Fig. 2 E). We also examined the specificity of the effect of CY-09 on NLRP3 activation and found that CY-09 had no effect on cytosolic double-stranded DNA–induced AIM2 inflammasome and $Salmonella$ infection–induced NLRC4 inflammasome activation (Fig. 2, F and G). In addition, CY-09 treatment had no effect on LPS-induced TNF-α production, pro–IL-1β, and NLRP3 expression (Fig. S1, A and B). LPS-induced priming could affect the ubiquitination status of NLRP3 and then regulated NLRP3 activation (Juliana et al., 2012), and we found that CY-09 had no effects on NLRP3 ubiquitination during LPS-induced priming (Fig. S1 C). Indeed, CY-09 could inhibit caspase-1 activation when treated just before nigericin stimulation in BMDMs (Fig. S1 D). These results suggest that CY-09 has no effect on LPS-induced priming in BMDMs. Consistent
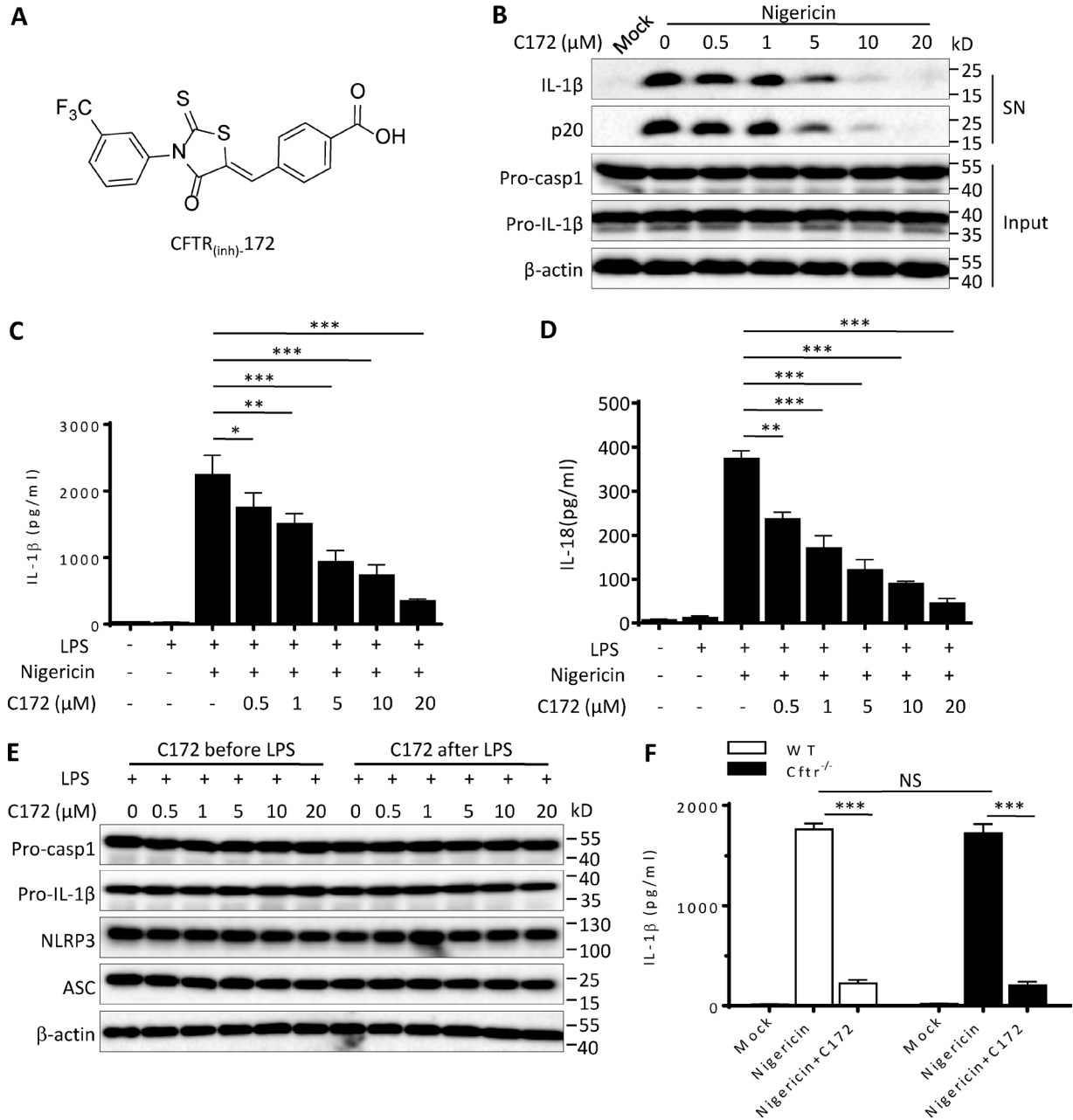
Figure 1. C172 inhibits NLRP3 activation via CFTR–independent manner. (A) C172 structure. (B) Immunoblot analysis of IL-1β and cleaved caspase-1 in culture supernatants (SN) of LPS-primed BMDMs treated with various doses (above lanes) of C172 and then stimulated with nigericin. (C and D) ELISA of IL-1β (C) and IL-18 (D) in supernatants from LPS-primed BMDMs treated with various doses (above lanes) of C172 and then stimulated with nigericin. (E) Immunoblot analysis of the indicated proteins in lysates from BMDMs treated with LPS for 3 h and stimulated with different doses of C172 for 30 min (C172 after LPS) or BMDMs treated with different doses of C172 for 30 min and then stimulated with LPS for 3 h (C172 before LPS). (F) ELISA of IL-1β in supernatants from LPS-primed WT or *Cftr*^{−/−} BMDMs that were treated with nigericin with or without the presence of C172 (20 μM). Data are from three independent experiments with biological duplicates in each (C, D, and F; mean and SEM of *n* = 6) or are representative of three independent experiments (B and E). Statistics were analyzed using an unpaired Student's *t* test: *, P < 0.05; **, P < 0.01; ***, P < 0.001.

with the inflammasome inhibition. CY-09 also blocked nigericin–induced BMDM death (Fig. S1 E).

A few compounds, including sulforaphane, isoliquiritigenin, BHB, flufenamic acid, mefenamic acid, parthe-nolide, BAY 11-7082, and MCC950, have been reported to inhibit NLRP3 inflammasome activation (Juliana et al., 2010; Honda et al., 2014; Youm et al., 2015; Daniels et al., 2016; Greaney et al., 2016); we thus compared the activity
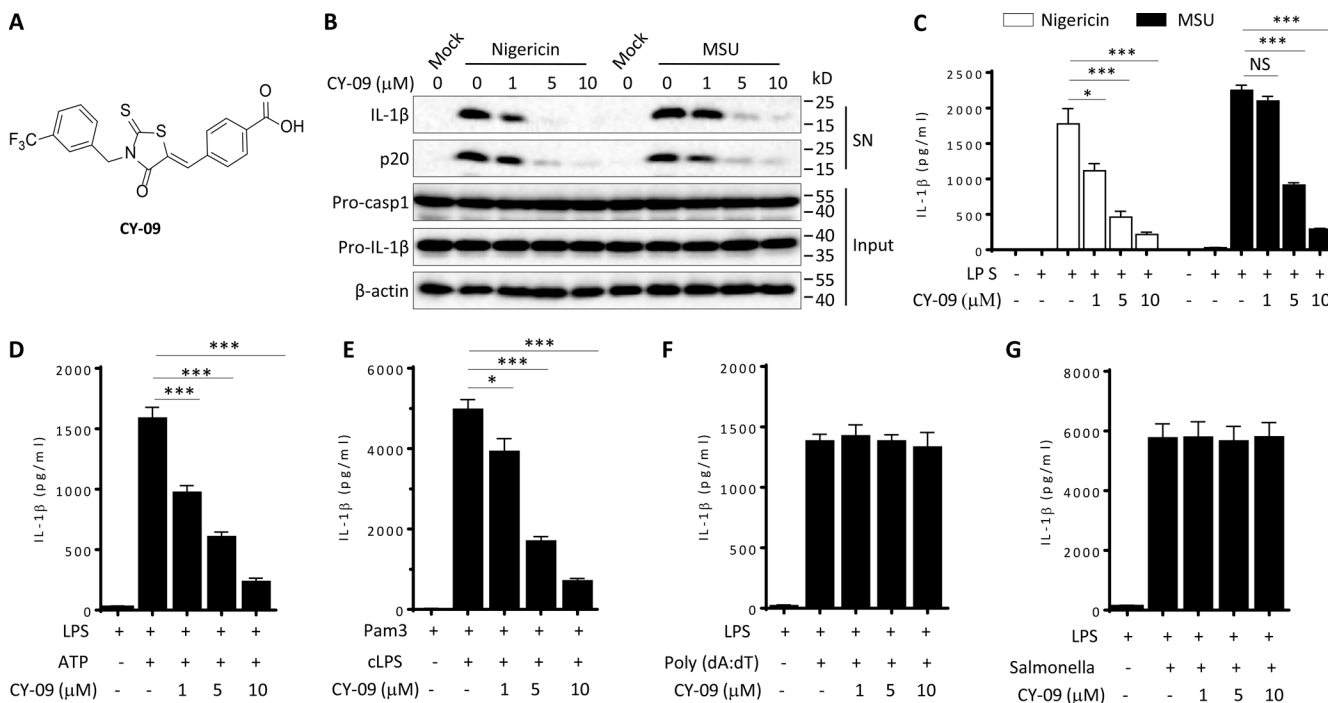
Figure 2. CY-09 blocks NLRP3 inflammasome activation. (A) CY-09 structure. (B) Immunoblot analysis of IL-1β and cleaved caspase-1 (p20) in culture supernatants (SN) of LPS-primed BMDMs treated with various doses (above lanes) of CY-09 and then stimulated with nigericin and immunoblot analysis of the precursors of IL-1β (pro–IL-1β) and caspase-1 (pro–caspase-1) in lysates of those cells (input). (C–G) ELISA of IL-1β in supernatants from LPS-primed BMDMs treated with various doses of CY-09 and then stimulated with nigericin, MSU (C), ATP (D), cytosolic LPS (E), cytosolic poly(dA:dT) (F), or *Salmonella* (G). Data are from three independent experiments with biological duplicates in each (C–G; mean and SEM of $n = 6$) or are representative of three independent experiments (B). Statistics were analyzed using an unpaired Student's t test: *, $P < 0.05$; ***, $P < 0.001$.

and specificity of these inhibitors with CY-09. Among these inhibitors, MCC950 showed the best inhibitory activity for NLRP3 inflammasome, while CY-09 had comparable activity with sulforaphane, isoliquiritigenin, parthenolide, and BAY 11-7082 (Fig. 3 A). Consistent with previous studies (Juliana et al., 2010; Greaney et al., 2016), sulforaphane and parthenolide could also inhibit AIM2 or NLRC4 inflammasome activation (Fig. 3, B and C), suggesting they are not specific NLRP3 inflammasome inhibitors. Previous studies have shown that sulforaphane, isoliquiritigenin, BHB, flufenamic acid, mefenamic acid, parthenolide, and BAY 11-7082 have inhibitory activity for NF-κB (Heiss et al., 2001; Yip et al., 2004; Honda et al., 2012; Strickson et al., 2013; Fu et al., 2015; Goldberg et al., 2017; Pongkorpsakol et al., 2017), we confirmed these results and found that they could suppress LPS-induced TNF-α production or pro–IL-1β expression when BMDMs were treated with these inhibitors before LPS stimulation (Fig. S2, A and B), suggesting that these inhibitors have broad anti-inflammatory activity. In contrast, CY-09 and MCC950 specifically inhibited NLRP3 inflammasome activation and had no effect on LPS-induced priming effects (Fig. 3 and Fig. S2). Thus, these results indicate that CY-09 is a specific inhibitor for NLRP3 inflammasome.

CY-09 inhibits NLRP3 oligomerization and inflammasome assembly

We then asked how CY-09 inhibited NLRP3 activation. ASC oligomerization is critical for the subsequent caspase-1 activation (Lu et al., 2014; Dick et al., 2016). We found that CY-09 treatment remarkably suppressed nigericin–induced ASC oligomerization (Fig. 4 A), indicating that CY-09 acts upstream of ASC oligomerization to inhibit the subsequent caspase-1 activation and IL-1β production. Mitochondria damage, represented as mitochondria fission, clustering and reactive oxygen species production, is proposed as an upstream signaling event of NLRP3 activation (Zhou et al., 2011). CY-09 treatment had little effects on nigericin–induced mitochondrial damage and reactive oxygen species production (Fig. 4 B), suggesting that CY-09 does not affect mitochondrial damage in NLRP3 inflammasome activation.

We next examined whether CY-09 inhibited potassium efflux, another upstream signaling event of NLRP3 activation (Pétrilli et al., 2007; Muñoz-Planillo et al., 2013). Nigericin induced a decrease of intracellular potassium dramatically in *Nlrp3*^{−/−} BMDMs, but this was not suppressed by CY-09 (Fig. 4 C), suggesting that it has no effect on potassium efflux during NLRP3 inflammasome activation. BHB could sup-
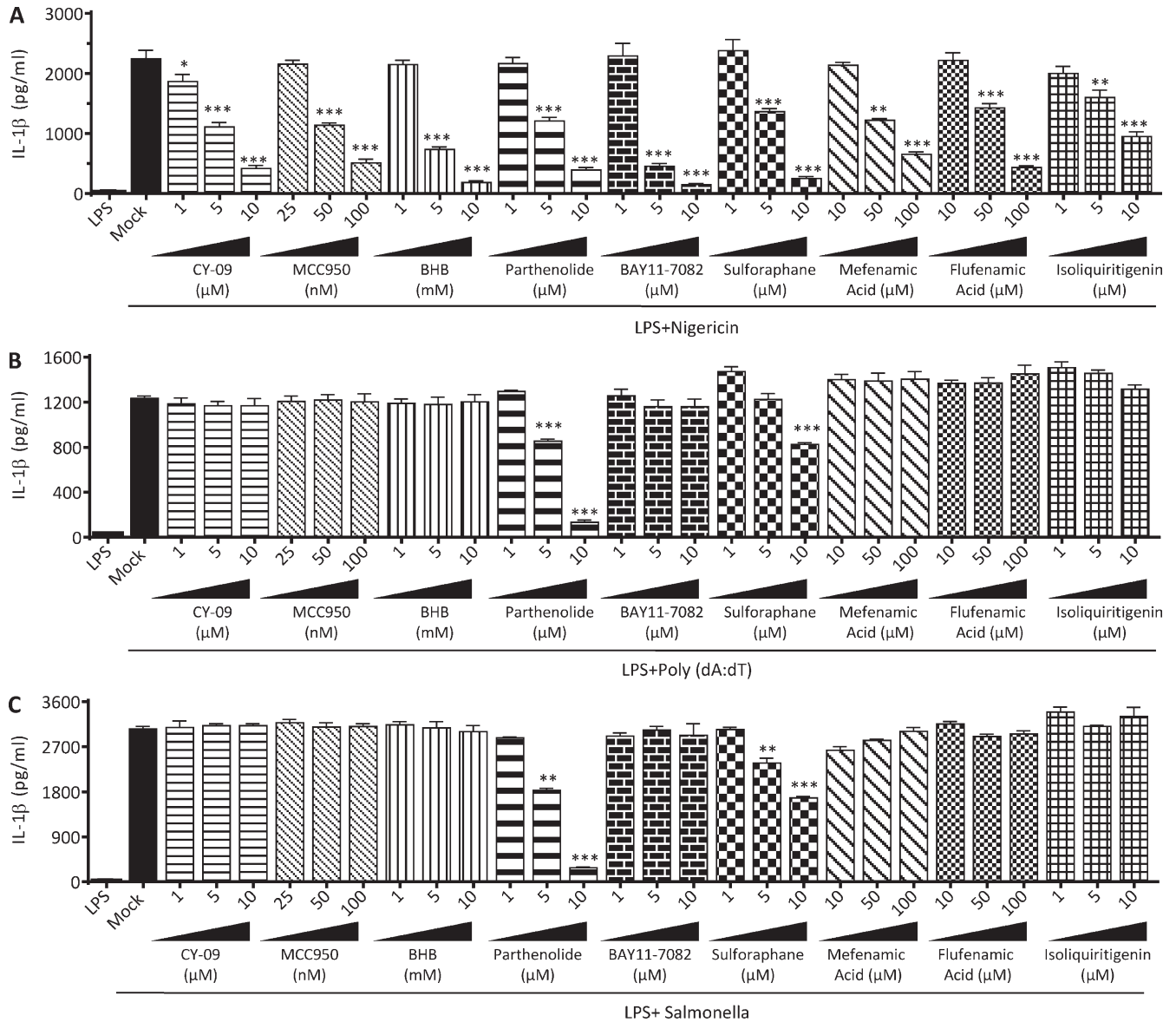
Figure 3. **Role of inhibitors on inflammasome activation.** (A–C) ELISA of IL-1β in supernatants from LPS-primed BMDMs treated with various doses of indicated inhibitors and then stimulated with nigericin (A), poly(dA:dT) (B), or *Salmonella* (C). Data are from three independent experiments with biological duplicates in each (mean and SEM of $n = 6$). Statistics were analyzed using an unpaired Student's *t* test: *, $P < 0.05$; **, $P < 0.01$; ***, $P < 0.001$.

press nigericin–induced potassium efflux, whereas MCC950 and flufenamic acid could not (Fig. 4 D).

In addition, volume-regulated anion channel–dependent chloride efflux has been proposed as another upstream signaling event for NLRP3 activation (Daniels et al., 2016). Consistent with this study, we found that flufenamic acid treatment blocked nigericin–induced decrease of intracellular chloride $Nlrp3^{-/-}$ BMDMs (Fig. 4 E). In contrast, CY-09 had no effect on nigericin–induced decrease of intracellular chloride (Fig. 4 E). MCC950 has shown strong inhibitory activity for NLRP3 inflammasome and beneficial effects in several mice models of NLRP3-related diseases (Coll et al.,

2015; Dempsey et al., 2017), but the mechanism is not well understood. Interestingly, we found that MCC950 could inhibit nigericin–induced chloride efflux in $Nlrp3^{-/-}$ BMDMs in a dose-dependent manner and correlated with its inhibitory activity for NLRP3 activation (Fig. 4 E), suggesting that MCC950 might target chloride efflux to suppress inflammasome activation.

We then examined whether CY-09 inhibited the formation of NLRP3 inflammasome complex. The two critical steps for NLRP3 inflammasome complex formation are NLRP3 oligomerization and recruitment of ASC to NLRP3 oligomers (Martinon et al., 2009; Davis et al., 2011). We
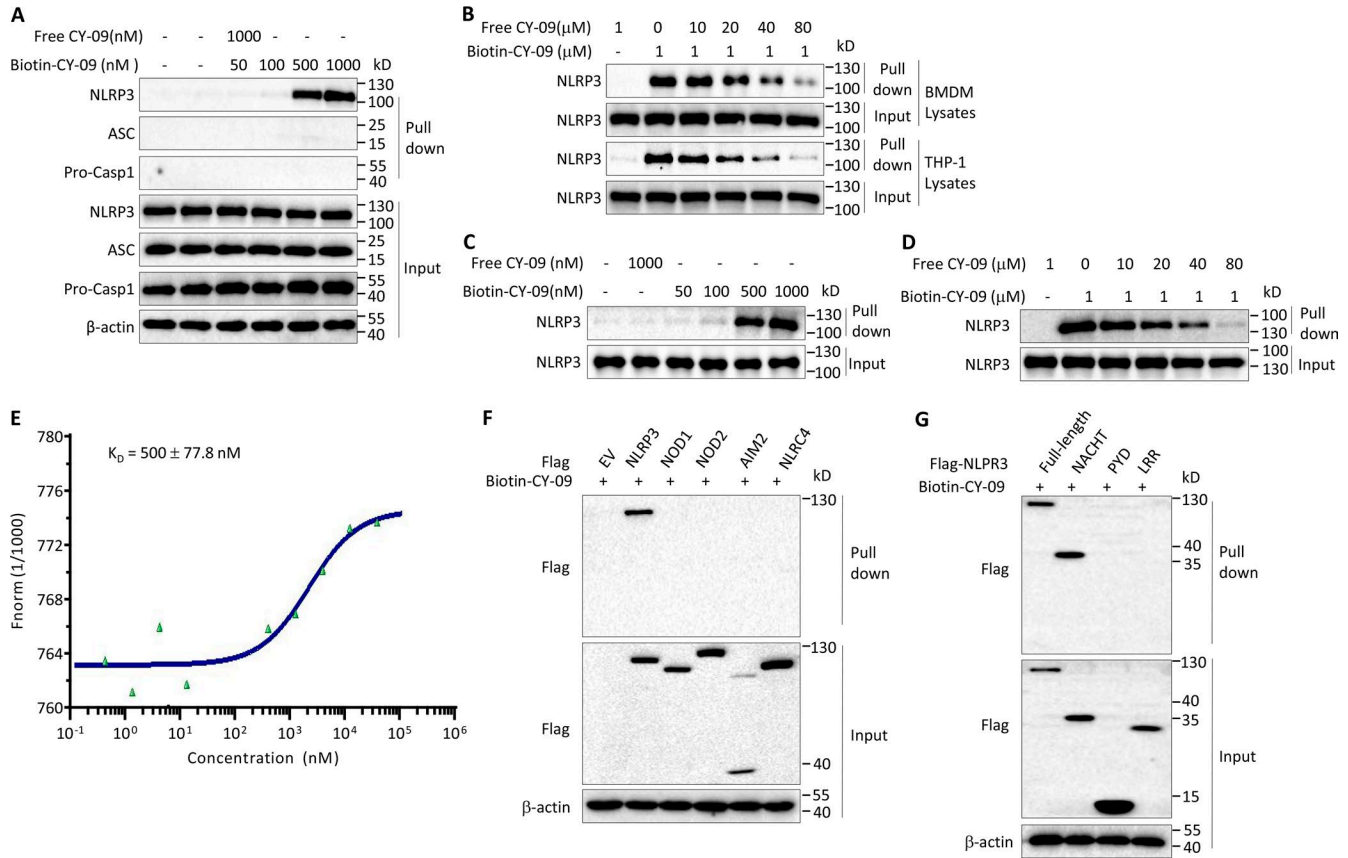
Figure 4. **CY–09 inhibits NLRP3 inflammasome assembly.** (A) Immunoblot analysis of ASC oligomerization in lysates of BMDMs treated with various doses (above lanes) of CY-09 and then stimulated with nigericin. SN, supernatants. (B) Confocal microscopy analysis in LPS-primed BMDMs treated with CY-09 (10 μM) and then stimulated with nigericin, followed by staining with MitoSOX and MitoTracker red. Nuclei were stained with DAPI. Bars, 10 μm. (C) Qualification of potassium efflux in LPS-primed BMDMs treated with different doses of CY-09 and then stimulated with nigericin. (D and E) Qualification of potassium (D) and chloride (E) efflux in LPS-primed BMDMs treated with different doses of indicated inhibitors and then stimulated with nigericin. (F) IP and immunoblot analysis of the interaction of Flag–NLRP3 and VSV–NLRP3 in the lysates of HEK-293T cells. (G) Immunoblot analysis of NLRP3 by SDD-AGE or SDS-PAGE assay in WT or $Nlrp3^{-/-}$ BMDMs treated with various doses of CY-09 and then stimulated with nigericin. (H) IP and immunoblot analysis of the interaction of endogenous NLRP3 and ASC in LPS-primed BMDMs treated with various doses (above lanes) of CY-09 and then stimulated with nigericin. Data are from three independent experiments with biological duplicates in each (C–E; mean and SEM of $n = 6$) or are representative of three independent experiments (A, B, and F–H). Statistics were analyzed using an unpaired Student's t test: *, $P < 0.05$; ***, $P < 0.001$.

examined whether CY-09 could prevent direct NLRP3–NLRP3 or NLRP3–ASC interactions. Indeed, we found that CY-09 treatment inhibited the interaction of Flag–NLRP3 and mCherry–NLRP3 in HEK-293T cells, suggesting that CY-09 blocks NLRP3 oligomerization (Fig. 4 F). The effect of CY-09 on the endogenous NLRP3 oligomerization was confirmed using semi–denaturing detergent agarose gel electrophoresis (SDD-AGE; Fig. 4 G), a method for detecting large protein oligomers in studying prions (Alberti et al., 2009; Hou et al., 2011). Moreover, CY-09 treatment suppressed nigericin-induced endogenous NLRP3–ASC interaction in BMDMs (Fig. 4 H). These results indicate that CY-09 inhibits inflammasome activation by blocking NLRP3 oligomerization and inflammasome assembly.

CY–09 directly binds to NLRP3 and inhibits its ATPase activity

Because CY-09 inhibited NLRP3 oligomerization, we next investigated whether CY-09 inhibited NLRP3 oligomerization by directly binding to NLRP3 protein. A synthesized biotinylated analogue of CY-09 (Fig. S3 A; biotin–CY-09) was used as an affinity reagent and incubated with cell lysates of LPS-primed BMDMs (Fig. 5 A) or PMA-differentiated THP-1 cells (Fig. S3 B). This compound was pulled down with streptavidin beads, and NLRP3 component proteins were detected by immunoblot analysis. The data showed that NLRP3, but not ASC or caspase-1, was pulled down by biotin–CY-09 (Fig. 5 A and Fig. S3 B). In addition, NEK7, another component of NLRP3 complex (He et al., 2016;

Figure 5. **CY-09 binds to the ATP-binding site of NLRP3 NACHT domain.** (A) Cell lysates of LPS-primed BMDMs were incubated with different concentrations of biotin–CY-09, which were then pulled down with streptavidin beads. (B) Cell lysates of LPS-primed BMDMs or PMA-differentiated THP-1 cells were incubated with biotin–CY-09 and different concentrations of free CY-09, which were then pulled down with streptavidin beads. (C) Purified human NLRP3 protein was incubated with different concentrations of biotin–CY-09 and then pulled down with streptavidin beads. (D) Purified human NLRP3 protein was incubated with biotin–CY-09 and different concentrations of free CY-09, which were then pulled down with streptavidin beads. (E) MST assay for the affinity between CY-09 and purified GFP-NLRP3 protein. (F and G) Cell lysates from HEK-293T cells transfected with Flag-tagged NLRP3, NOD1, NOD2, AIM2, NLRC4, NLRP3–LRR, NLPR3–NACHT, or NLRP3–PYD constructs were incubated with indicated concentration of biotin–CY-09, which were then pulled down with streptavidin beads. Data are representative of three independent experiments.

Schmid-Burgk et al., 2016; Shi et al., 2016), was also not pulled down (Fig. S3 C). Moreover, the pull-down of NLRP3 by biotin–CY-09 could be competed off by free CY-09 (Fig. 5 B). To determine whether CY-09 interacts with NLRP3 directly, purified human NLRP3 protein was incubated with biotin–CY-09, and NLRP3 could be pulled down with biotin–CY-09 and competed off by free CY-09 (Fig. 5, C and D; and Fig. S3 D), confirming that CY-09 directly interacts with NLRP3. To more precisely validate CY-09 as a potential NLRP3 inhibitor, we used microscale thermophoresis (MST) assay to measure the direct interaction between CY-09 and GFP-NLRP3. The equilibrium dissociation constant (K_D) between CY-09 and purified GFP-NLRP3 was about 500 nM (Fig. 5 E and Fig. S3 E).

We next studied whether CY-09 bound to other innate immune sensors. Flag-tagged NLRP3, NOD1, NOD2, AIM2, and NLRC4 were overexpressed in HEK-293T cells, and the cell lysates were then incubated with biotin–CY-09.

The results showed that only NLRP3 could be pulled down (Fig. 5 F), suggesting that CY-09 specifically binds with NLRP3. NLRP3 contains three functional domains, LRR, NACHT, and PYD. We then studied which domain was responsible for the binding between NLRP3 and CY-09, and the results showed that only NACHT domain of NLRP3 bound CY-09 (Fig. 5 G). These results indicate that CY-09 directly binds to the NACHT domain of NLRP3.

Previous results have shown that the ATPase activity of NLRP3 NACHT domain is essential for the oligomerization of NLRP3 (Duncan et al., 2007); we thus tested whether CY-09 could affect the ATPase activity of NLRP3. The results showed that CY-09 inhibited the ATPase activity of purified NLRP3 at doses of 0.1–1 μM, as measured by the release of free phosphate (Fig. 6 A). The inhibitory effect of CY-09 on NLRP3 ATPase activity was specific because it had no effect on the ATPase activity of purified NLRC4, NLRP1, NOD2, or RIG-I (Fig. 6 B and Fig. S3 D).
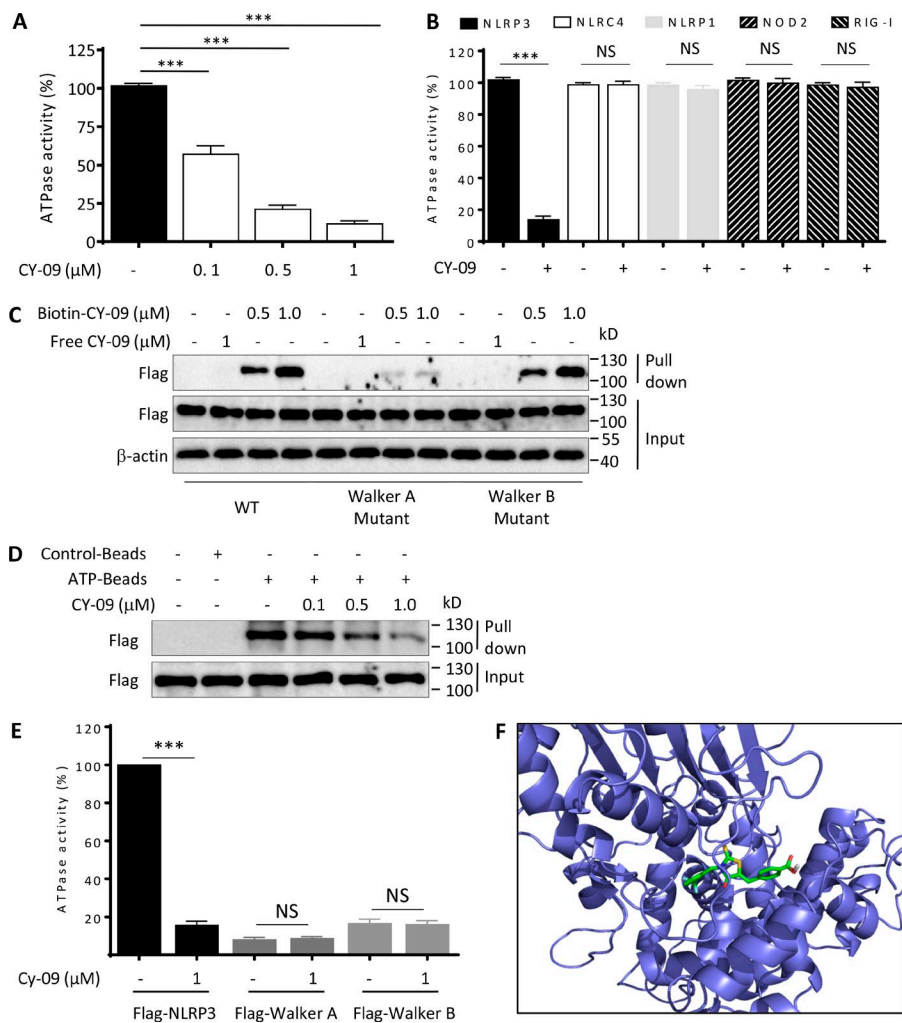
Figure 6. **CY-09 inhibits NLRP3 ATPase activity.** (A) ATPase activity assay for purified human NLRP3 in the presence of different concentrations of CY-09. (B) ATPase activity assay for purified Flag–NLRP3, NLRC4, NLRP1, NOD2 or RIG-I with or without presence of CY-09 (1 µM). (C) Cell lysates from HEK-293T cells transfected with Flag-tagged WT NLRP3 or NLRP3 constructs with Walker A or Walker B motif mutation were incubated with different concentrations of biotin–CY-09 and then pulled down with streptavidin beads. (D) ATP-binding assay for purified Flag–NLRP3 in the presence of different concentrations of CY-09. (E) ATPase activity assay for purified Flag–NLRP3 or mutants with or without presence of CY-09 (1 µM). (F) Docking complex of NLRP3 with CY-09. CY-09 is shown in sticks and colored green, while NLRP3 is shown in cartoon and colored light blue. Data are from three independent experiments with biological duplicates in each (A, B, and E; mean and SEM of $n = 6$) or are representative of two or three independent experiments (C and D). Statistics were analyzed using an unpaired Student's t test: ***, $P < 0.001$.

We also studied how CY-09 inhibited the ATPase activity of NLRP3. NLRP3 contains two motifs in NACHT domain that are important for its ATPase activity. Walker A motif is important for ATP binding, while Walker B motif is necessary for ATPase activity (MacDonald et al., 2013). Although both mutants had no ATPase activity (Fig. 6 E), we found that mutation of Walker A motif of NLRP3 impaired the binding of CY-09 to NLRP3, but mutation of Walker B motif had no effect (Fig. 6 C). Consistent with this, CY-09 competed off the binding of purified NLRP3 with ATP in a dose–dependent manner (Fig. 6 D). These results suggest that CY-09 binds to the Walker A motif of NLRP3 to abolish the ATP binding of NLRP3 and then blocks its ATPase activity. To further evaluate how CY-09 inhibited NLRP3 ATPase activity, we performed human NLRP3 homology modeling and docking calculation using a chain from crystal structure of rabbit NOD2 bound with ADP (Protein Data Bank accession no. 5IRM) as a template structure. The results showed that CY-09 was readily docked into the ATP-binding pocket formed by its NACHT domain (Fig. 6 F). Thus, these results suggest that CY-09 may bind to the ATP-binding site

of NLRP3 and then inhibit NLRP3 ATPase and subsequent NLRP3 oligomerization and activation.

CY-09 inhibits NLRP3 activation in vivo and prevents neonatal lethality in a mouse model of CAPS

We next examined the pharmacokinetic profile of this compound before assessing the therapeutic potential of CY-09 in vivo. The metabolic stability of CY-09 was first evaluated using human and mouse liver microsomes, exhibiting favorable stability with the half-life >145 min for both human and mouse microsomes (Table S1). CY-09 was tested against the five major cytochrome P450 enzymes 1A2, 2C9, 2C19, 2D6, and 3A4 with half maximal inhibitory concentration (IC_{50}) values of 18.9, 8.18, >50, >50, and 26.0 µM, respectively (Table S2), which exhibited low risk of drug–drug interactions. To evaluate the potential for cardiotoxicity, we examined the effect of CY-09 on the human ether-a-go-go (hERG) potassium channel using the automated patch clamp method (QPatch[HTX]), and CY-09 showed no activity for hERG at 10 µM (Table S3). Then, the pharmacokinetic properties of CY-09 were further evaluated in C57BL/6J mice
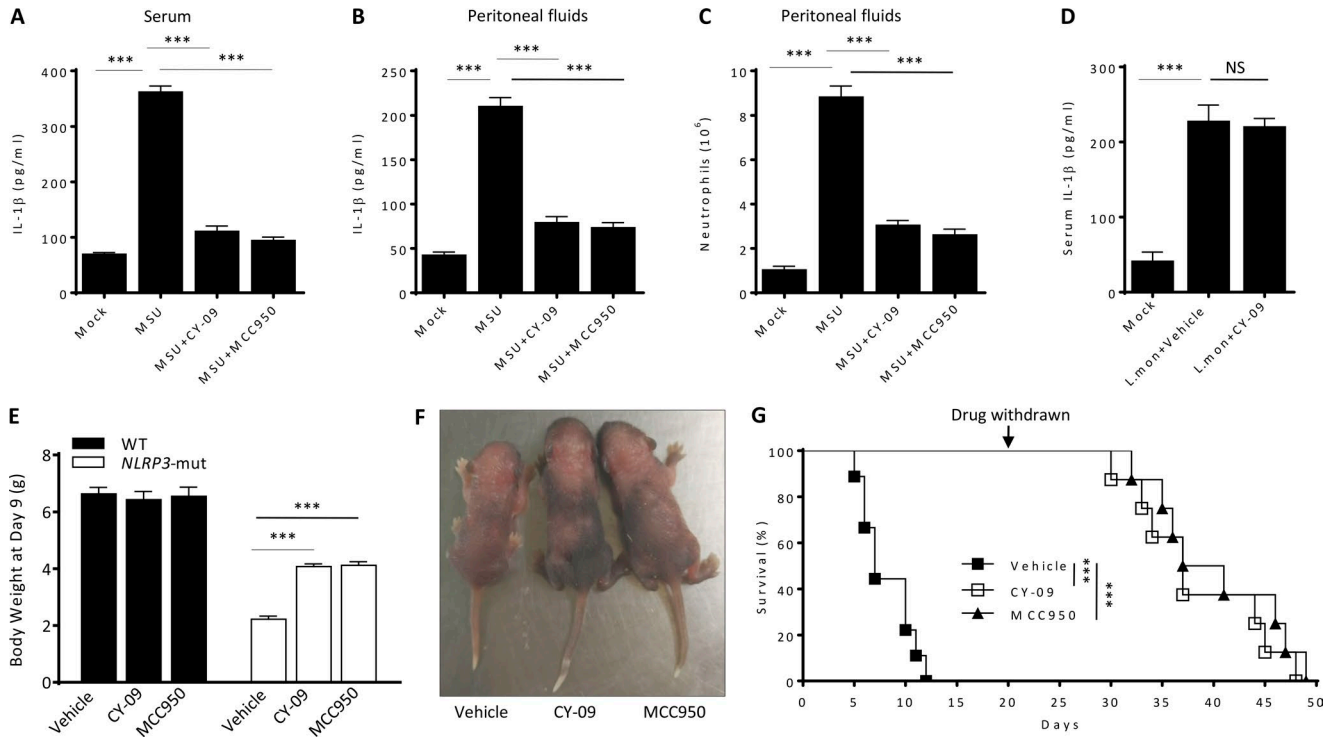
Figure 7. **CY–09 inhibits NLRP3 activation in MSU–induced peritonitis and a mouse model of MWS.** (A and B) ELISA of IL-1β in the serum (A) or peritoneal cavity (B) of C57BL/6J mice intraperitoneally injected with MSU (1 mg/mouse) with or without CY-09 (40 mg/kg) or MCC950 (40 mg/kg). Data are representative of two independent experiments (mean and SEM of n = 6). (C) FACS analysis of neutrophil numbers in the peritoneal cavity of C57BL/6J mice intraperitoneally injected with MSU (1 mg/mouse) with or without CY-09 (40 mg/kg) or MCC950 (40 mg/kg). Data are representative of two independent experiments (mean and SEM of n = 6). (D) ELISA of IL-1β in serum of $Nlrp3^{-/-}$ mice intraperitoneally injected with $L.$ $monocytogenes$ ($L.mon$; 5 × 10^{6}) for 8 h with or without CY-09 (40 mg/kg). (E) Weight of WT or $Nlrp3A^{350VneoR}$ crossed with LysM-Cre mice ($NLRP3$-mut) treated with CY-09 or MCC950 at day 9. Data are representative of two independent experiments (mean and SEM). WT vehicle, WT CY-09, and WT MCC950 (n = 6), $NLRP3$-mut vehicle (n = 4), $NLRP3$-mut CY-09 or MCC950 (n = 5). (F) $NLRP3$-mut mice treated with CY-09 or MCC950 on day 9. (G) Survival of $NLRP3$-mut mice treated with vehicle or CY-09 up to day 49 (CY-09 withdrawn at day 25). Data are representative of two independent experiments. CY-09 group (n = 8), MCC950 group (n = 8), vehicle group (n = 9). Statistics were analyzed using an unpaired Student's t test (A–E) or a generalized Wilcoxon test (G): ***, P < 0.001.

administered a single i.v. or oral dose. CY-09 exhibited favorable pharmacokinetics, with a half-life of 2.4 h, an area under the curve of 8,232 (h·ng)/ml, and bioavailability of 72% (Table S4). With these data in hand, the in vivo efficacy of CY-09 was then evaluated.

Intraperitoneal injection of MSU elicited an NLRP3-dependent peritonitis characterized by IL-1β production and massive neutrophil influx (Martinon et al., 2006). Comparable with MCC950, CY-09 treatment in vivo efficiently suppressed MSU injection–induced IL-1β production and neutrophil influx (Fig. 7, A–C), suggesting that CY-09 can block MSU-induced NLRP3 inflammasome activation in vivo. In contrast, CY-09 had no effect on *Listeria monocytogenes* infection–induced IL-1β production in $Nlrp3^{-/-}$ mice, suggesting that CY-09 has no inhibitory activity for AIM2 inflammasome activation in vivo (Fig. 7 D).

Mutations in the gene coding for NLRP3 (such as A352V) have been shown to be associated with Muckle-Wells syndrome (MWS), which is an autoinflammatory syndrome characterized by excessive secretion of IL-1β (Ting et

al., 2006). *NLRP3* mutant mice with specific expression of MWS-associated mutation *Nlrp3* (A350V*neoR*) in the myeloid lineage die in the neonatal period and have increased concentrations of circulating IL-1β and IL-18 (Brydges et al., 2009). We then administered CY-09 to *NLRP3* mutant mice and found that CY-09-treated *NLRP3* mutant mice had increased body weight at day 9 compared with the control group (Fig. 7, E and F). CY-09 treatment also increased the survival of *NLRP3* mutant mice up to days 30–48 even after treatment was stopped at day 25 (Fig. 7 G), suggesting that CY-09 can suppress the lethal inflammation caused by *NLRP3* mutation. Collectively, these results suggest that CY-09 is active in vivo and can prevent NLRP3-dependent acute inflammation.

CY–09 reverses metabolic disorders in diabetic mice by inhibition of NLRP3-dependent inflammation

In addition to acute inflammation, NLRP3 inflammasome has been regarded as an important contributor for the chronic inflammation associated complex diseases, including T2D, Alzheimer's disease, and atherosclerosis (Martinon et al.,
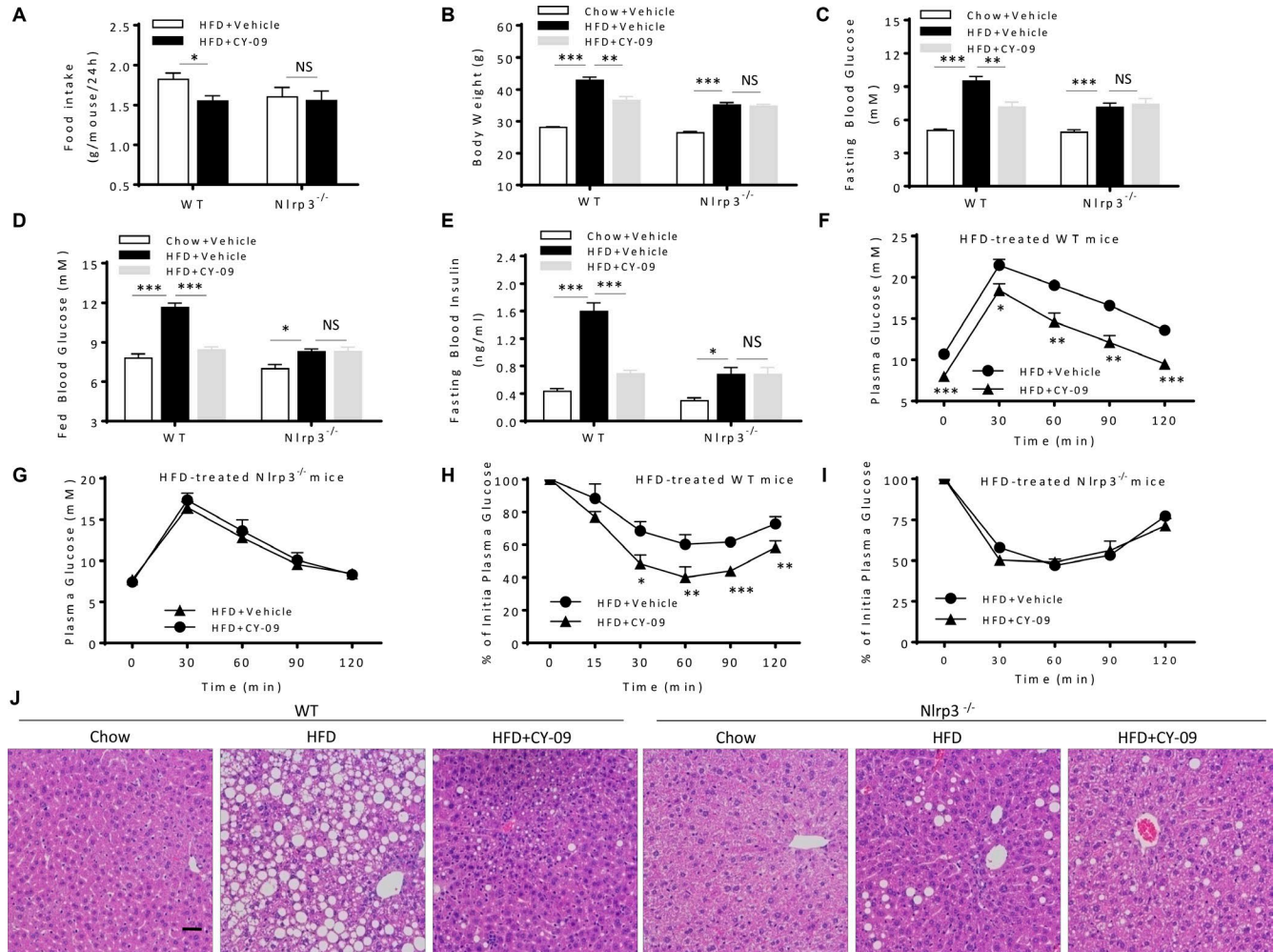
Figure 8. **Treatment of metabolic disorders in HFD–induced diabetic mice with CY–09.** (A and B) Food intake and body weight change of WT or $Nlrp3^{-/-}$ mice that were first fed with an HFD for 14 wk and then treated with CY-09 for 6 wk. $n = 6$–8 per group. (C and D) Fasting (C) or fed (D) blood glucose concentrations at week 6 in the mice described in A. $n = 6$–8. (E) Fasting blood insulin concentration at week 6 in the mice described in A. $n = 6$–8 per group. (F–I) Glucose tolerance test (F and H) and insulin tolerance test (G and I) performed at week 6 in the mice described in A. $n = 6$–8 per group. (J) Representative H&E staining of liver sections of WT or $Nlrp3^{-/-}$ mice that were first fed with an HFD for 14 wk and then treated with CY-09 for 6 wk. Bar, 50 µm; $n = 6$. Data are shown as mean and SEM and are representative of two independent experiments. Statistics were analyzed using an unpaired Student's t test (A–E) or two-way ANOVA for (F–I): *, $P < 0.05$; **, $P < 0.01$; ***, $P < 0.001$.

2006; Duewell et al., 2010; Masters et al., 2010; Zhou et al., 2010; Wen et al., 2011; Heneka et al., 2012; Lamkanfi and Dixit, 2012; Broderick et al., 2015), suggesting the possibility to treat these diseases by inhibition of NLRP3 inflammasome-dependent inflammation. We then tested whether CY-09 treatment was effective in reversing metabolic disorders in diabetic mice. The WT mice and $Nlrp3^{-/-}$ mice were fed with a high-fat diet (HFD) for 14 wk and then treated with CY-09 once a day at a dose of 2.5 mg/kg for 6 wk. CY-09 treatment reduced food intake and weight gain significantly compared with the control group (Fig. 8, A and B). We also found that CY-09 treatment significantly reduced fasting or basal blood glucose concentrations in HFD-treated WT mice (Fig. 8, C and D). The insulin level in blood was also de-

creased by CY-09 administration (Fig. 8 E). In addition, the CY-09-treated mice showed better insulin sensitivity than controls (Fig. 8, F and H). However, the beneficial effects of CY-09 on metabolic disorders were not observed in HFD-fed $Nlrp3^{-/-}$ mice (Fig. 8, A–E, G, and I), suggesting that CY-09 alleviates diabetic symptoms via inhibition of NLRP3 inflammasome. We also evaluated whether CY-09 treatment had any effect on HFD-induced hepatic steatosis and found that mice treated with CY-09 showed much less intracellular lipid accumulation in the liver compared with control mice (Fig. 8 J). Thus, these results indicate that CY-09 treatment can reverse NLRP3-dependent metabolic disorders in diabetic mice.

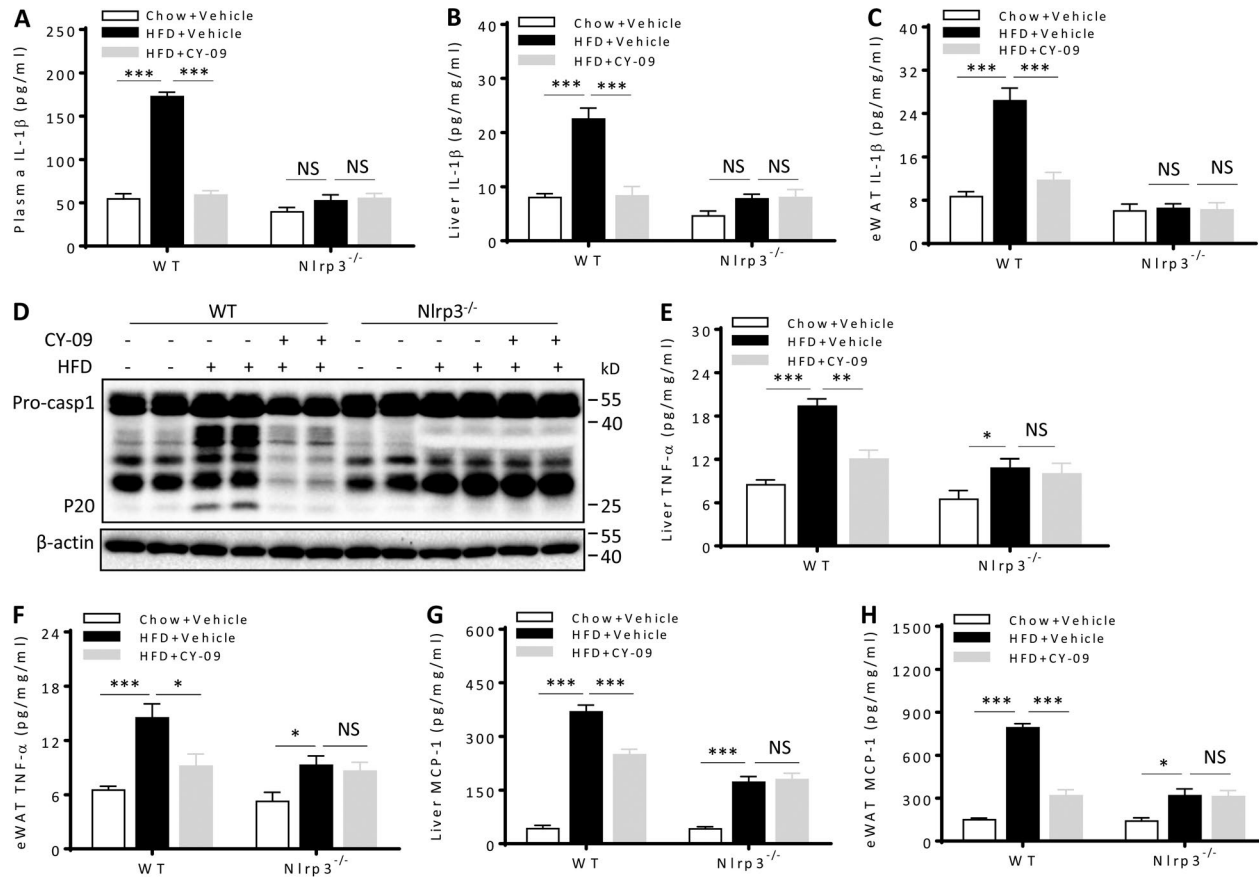In diabetic mice, NLRP3-dependent low-grade meta-inflammation in metabolic organs, such as liver or adipose

Figure 9. CY–09 suppresses NLRP3–dependent metainflammation in diabetic mice. (A–H) WT or *Nlrp3*^{-/-} mice were first fed with an HFD for 14 wk and then treated with CY-09 for 6 wk. Plasma IL-1β (A) was assessed by ELISA. Liver (B, E, and G) and white adipose tissue (WAT; C, F, and H) were isolated and cultured for 24 h, and supernatants were analyzed by ELISA for IL-1β (B and C), TNF-α (E and F), or monocyte chemoattractant protein 1 (G and H). Caspase-1 activation in WAT was analyzed by immunoblot as indicated (D). *n* = 6–8 per group. Data are shown as mean and SEM and are representative of two independent experiments. Statistics were analyzed using an unpaired Student's *t* test: *, P < 0.05; **, P < 0.01; ***, P < 0.001.

tissue, is critical for the development of T2D (Stienstra et al., 2010; Yan et al., 2013). To further confirm that CY-09 reverses metabolic disorders through inhibition of NLRP3 activation, we examined whether CY-09 treatment inhibited NLRP3 inflammasome activation and metainflammation in diabetic mice. As expected, NLRP3-dependent IL-1β production in serum, liver, or adipose tissues of HFD-treated mice was impaired by CY-09 treatment (Fig. 9, A–C). The caspase-1 cleavage observed in adipose tissue of HFD-treated mice was also suppressed by CY-09 (Fig. 9 D), indicating that CY-09 treatment can inhibit metabolic stress-induced inflammasome activation in vivo. In addition, the production of TNF-α and MCP-1, which are inflammasome-independent cytokines, were also decreased in HFD-treated mice (Fig. 9, E–H), which was consistent with the observation in *Nlrp3*^{-/-} mice. These results suggest that CY-09 treatment not only blocks metabolic stress-induced NLRP3 inflammasome activation but also suppresses NLRP3-dependent metainflammation. Thus, these results indicate that CY-09

can treat metabolic disorders by inhibition of NLRP3 inflammasome in diabetic mice.

We also examined the effects of CY-09 on the metabolic parameters of normal lean mice. C57BL/6J mice fed with a normal diet were treated with CY-09 once a day at a dose of 2.5 mg/kg for 9 wk, and the results revealed that CY-09 treatment had no effect on the metabolic parameters and serum chemistry (Fig. S4).

CY-09 is active ex vivo for cells from healthy human or gouty patients

We next examined whether CY-09 was effective for human cells. First, we found that CY-09 could efficiently inhibit nigericin-induced NLRP3 inflammasome activation in human THP-1 cells (Fig. 10 A). Moreover, nigericin-induced caspase-1 activation and IL-1β production in human peripheral blood mononuclear cells (PBMCs) could also be suppressed by CY-09 in a dose-dependent manner (Fig. 10, B and C). In contrast, CY-09 had no effect on TNF-α produc-
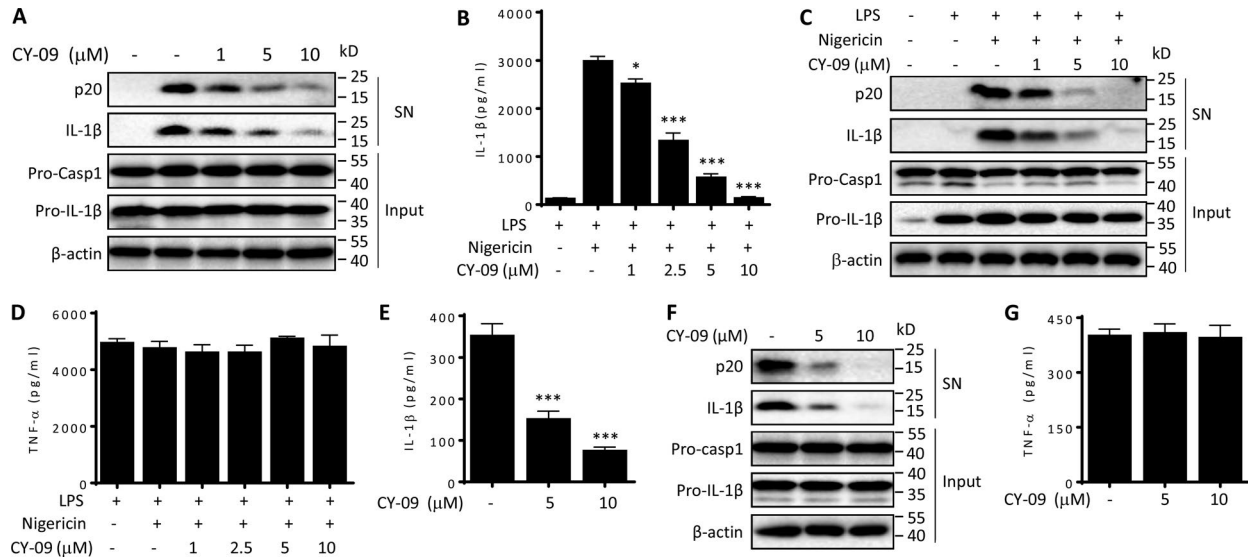
Figure 10. **CY-09 is active for cells from healthy humans or patients with gout.** (A) Immunoblot analysis of IL-1β and cleaved caspase-1 (p20) in culture supernatants (SN) of PMA-differentiated THP-1 cells treated with various doses (above lanes) of CY-09 and then stimulated with nigericin. (B–D) ELISA of IL-1β (B), TNF-α (D), or immunoblot analysis (C) of IL-1β and cleaved caspase-1 (p20) in supernatants from LPS-primed PBMCs, treated with various doses of CY-09 for 1 h and then stimulated with nigericin for 30 min. (E–G) ELISA of IL-1β (E), TNF-α (G), and immunoblot analysis (F) of IL-1β and cleaved caspase-1 (p20) in supernatants from SFCs isolated from an individual with gout, treated with various doses of CY-09 for 20 h. The SFCs isolated from five patients were analyzed, and the data are expressed as mean and SEM and are representative of five independent experiments. Statistics were analyzed using an unpaired Student's *t* test: *, $P < 0.05$; ***, $P < 0.001$.

tion (Fig. 10 D). Thus, these results suggest that CY-09 can prevent NLRP3 activation in human cells.

We then tested whether CY-09 had an effect on the preactivated NLRP3 inflammasome on cells from patients with abnormal NLRP3 activation. Gout is an inflammatory arthritis caused by precipitation of MSU in joints and bursal tissues of individuals with hyperuricemia (McQueen et al., 2012). NLRP3 inflammasome plays a critical role in MSU-induced inflammation, and clinical studies have demonstrated efficacy of IL-1 inhibitors in the treatment of patients with acute and chronic gout (Martinon et al., 2006; McGonagle et al., 2007; So et al., 2007; Terkeltaub et al., 2009; Jesus and Goldbach-Mansky, 2014). As expected, when freshly isolated synovial fluid cells (SFCs) from a patient with gout were incubated without the stimulation of NLRP3 agonists, IL-1β secretion and caspase-1 processing could be detected in the culture supernatants (Fig. 10, E and F). However, when these cells were incubated with the presence of CY-09, the caspase-1 activation and IL-1β production were inhibited in a dose-dependent manner (Fig. 10, E and F). In contrast, the production of inflammasome-independent cytokine TNF-α was not affected by CY-09 treatment (Fig. 10 G). SFCs from another four individuals with gout were also found to be sensitive to CY-09 inhibition (Fig. S5). Thus, these results indicate that CY-09 can suppress the preactivated NLRP3 inflammasome in SFCs from patients and suggest that CY-09 or its analogues might be used to control NLRP3-driven diseases in clinics.

DISCUSSION

In this study, we describe a potent, selective, and direct inhibitor of NLRP3 with remarkable inhibitory activity for NLRP3 inflammasome in mice in vivo and in human cells ex vivo. CY-09 will serve as a versatile tool to pharmacologically interrogate NLRP3 biology and study its role in inflammatory diseases.

A few compounds have shown potent inhibitory activity for the NLRP3 inflammasome and have been tested in animal models, but the unspecific effects of these compounds have limited their clinical potential. The inhibitory effects of sulforaphane on AIM2 or NLRC4 inflammasome suggest that it might impair the role of these inflammasomes in host defense (Greaney et al., 2016). The broad anti-inflammatory activity of sulforaphane, isoliquiritigenin, BHB, parthenolide, BAY 11-7082, and INF39 (Heiss et al., 2001; Yip et al., 2004; Honda et al., 2012; Strickson et al., 2013; Fu et al., 2015; Cocco et al., 2017) suggests that these compounds might cause immunosuppressive side effects and increase the risk for infection. The effects of flufenamic acid and mefenamic acid on chloride efflux and BHB on potassium efflux indicate that these compounds target the upstream signaling event of NLRP3 and have other unavoidable biological activities (Youm et al., 2015; Daniels et al., 2016). MCC950 has shown strong inhibitory activity and beneficial effects in several mice models of NLRP3-related diseases (Coll et al., 2015; Dempsey et al., 2017), but the mechanism is not understood. Here we showed that MCC950 could block NLRP3 agonist–induced chloride

efflux, a proposed upstream signaling event of NLRP3 activation (Daniels et al., 2016), suggesting that it might target the volume-regulated anion channel or other chloride channels to inhibit NLRP3 inflammasome activation and might have unspecific effects. Here we describe CY-09 as a specific NLRP3 inflammasome inhibitor that directly targeted NLRP3 itself and found that CY-09 had remarkable preventive or therapeutic effects on the mice models of CAPS, T2D, and gout. Thus, our study describes a direct and specific NLRP3 inhibitor with the potential to treat NLRP3-driven diseases.

Our results demonstrate that pharmacological inhibition of NLRP3 ATPase activity is efficient to treat NLRP3-driven diseases. Previous studies have reported that MNS, parthenolide, BAY 11-7082, and INF39 can inhibit the ATPase activity of NLRP3 and show inhibitory activity for NLRP3 inflammasome in vitro. However, these compounds are not specific NLRP3 inhibitors and have multiple biological activities, such as the inhibitory activity for tyrosine kinases or NF-κB signaling pathway (Yip et al., 2004; Wang et al., 2006; Strickson et al., 2013; Cocco et al., 2017). In addition, MNS, parthenolide, and BAY 11-7082 have not been tested in vivo in the animal models of NLRP3-driven diseases. CY-09 directly bound to the NACHT domain of NLRP3 and inhibited its ATPase activity, which is essential for NLRP3 oligomerization and inflammasome assembly (Duncan et al., 2007). Furthermore, the mutation of Walker A motif in the NACHT domain, which is required for ATP binding to NLRP3 (MacDonald et al., 2013), impaired the ability of CY-09 binding to NLRP3. In addition, our results clearly demonstrate that CY-09 competes with ATP to bind to NLRP3 and inhibits its ATPase activity and the subsequent NLRP3 oligomerization and inflammasome assembly. Importantly, our results show that suppression of NLRP3 ATPase activity by CY-09 has remarkable effects to reduce NLRP3 inflammasome activation and symptoms in mice models of T2D and CAPS. Thus, our results suggest the ATPase activity could be targeted to screen drug candidates for treatment of NLRP3-drive diseases.

The current available clinical treatment for NLRP3-related diseases is the use of agents that target IL-1β, but targeting NLRP3 itself with small-molecule inhibitors with high specificity, such as CY-09, might have certain advantages. In the CAPS mouse model, CY-09 was effective to prevent lethality, but blocking IL-1β alone could not (Brydges et al., 2009). The possible reason is that the IL-18 production or pyroptosis caused by inflammasome activation might also contribute to the pathology. In addition, IL-1β is also produced by other inflammasomes or in an inflammasome-independent way (Davis et al., 2011; Netea et al., 2015), so inhibition of NLRP3 itself might have less immunosuppressive side effects than blockade of IL-1β. Indeed, our results showed that CY-09 had no effect on AIM2 or NLRC4 inflammasomes, suggesting that CY-09 might not impair the role of these inflammasomes in host defense. Moreover, the small-molecule compounds are in general more cost effective than biological agents (Fautrel, 2012).

T2D is characterized by insulin resistance and hyperglycemia and can cause several complications, including nerve and kidney damage. However, the drugs available currently are not effective in correcting the underlying cause of insulin resistance, and most patients need pharmacotherapy for the rest of their lives (Nathan et al., 2009; Qaseem et al., 2012). Our study demonstrates that inhibition of NLRP3-dependent metainflammation by CY-09 is efficient to reverse the metabolic disorders in diabetic mice. CY-09 treatment had remarkable beneficial effects for metainflammation, hyperglycemia, and insulin resistance in diabetic mice. Thus, this study suggests that correcting NLRP3-dependent metainflammation might be an effective approach to treat T2D. Considering the role of NLRP3-dependent inflammation in the progression of gout, Alzheimer's disease, and atherosclerosis, CY-09 or its derivatives could be used for the development of new NLRP3-targeted therapeutics for these diseases.

MATERIALS AND METHODS

Mice

C57BL/6J mice at the age of 6 wk were purchased from the Model Animal Research Center of Nanjing University. $Nlrp3^{-/-}$, $Cftr^{-/-}$, and $Nlrp3^{A350VneoR}$ mice were described previously (Snouwaert et al., 1992; Martinon et al., 2006; Brydges et al., 2009). LysM-cre mice (B6.129P2-$Lyz2^{tm1(cre)Ifo}$/J) were from Jackson Laboratory. Mice were housed in a standard, pathogen-free animal facility under a 12-h light/dark cycle at 22–24°C with unrestricted access to food and water for the duration of the experiment except during fasting tests (no more than 16 h). All animal experimental protocols were reviewed and approved by the Animal Care Committee of the University of Science and Technology of China.

Chemical synthesis and formulation

Unless otherwise noted, reagents and solvents were obtained from a commercial supplier and were used without further purification. Reactions were monitored by thin-layer chromatography and were visualized with UV light. Removal of solvents was conducted by using a rotary evaporator, and residual solvent was removed from nonvolatile compounds using a vacuum manifold maintained at 1 torr. Chromatography was performed on ISCO CombiFlashRf 200 with prepacked silica-gel cartridges (RediSepRf Gold High Performance). Preparative high-pressure liquid chromatography was performed on a Waters Symmetry C18 column (19 × 50 mm, 5 μM) using a gradient of 5%–95% methanol in water containing 0.1% trifluoacetic acid over 8 min (10-min run time) at a flow rate of 20 ml/min. ^{1}H nuclear magnetic resonance (NMR) and ^{13}C NMR spectra were obtained on a BrukerUltrashield Plus-600 (600-MHz) spectrometer. Chemical shifts are reported in parts per million (δ) relative to residual undeuterated solvent as an internal reference. Coupling constants (J) are reported in hertz. Spin multiplicities are described as s (singlet), brs (broad singlet), t (triplet), q (quartet), and m (multiplet). Purities of

assayed compounds were in all cases >95%, as determined by reverse-phase high-performance liquid chromatographic analysis. C172 and CY-09 were prepared according to a reported procedure (Sonawane and Verkman, 2008). With the formulation of DMA:EL:HP-β-CD (10%, wt/vol) = 5:5:90 (vol/vol/v), CY-09 achieved a concentration of 1 mg/ml at pH 7.4. Using the formulation of DMSO:Solutol HS 15:saline = 10%:10%:80% (vol/vol/v), CY-09 reached a concentration of 5 mg/ml at pH 9.0. For the in vivo experiments, CY-09 was formulated in a vehicle containing 10% DMSO, 10% Solutol HS 15, and 80% saline.

C172
^{1}H NMR (600 MHz, DMSO-d_6) δ 8.12–8.08 (m, 2H), 7.98–7.96 (brs, 1H), 7.92 (d, J = 8.4 Hz, 1H), 7.90 (s, 1H), 7.85–7.79 (m, 4H); ^{13}C NMR (150 MHz, DMSO-d_6) δ 193.85, 166.72, 166.60, 136.77, 135.89, 133.32, 132.34, 131.23, 130.65, 130.58, 130.22, 130.05 (q, J = 31.5 Hz), 126.42 (q, J = 4.5 Hz), 126.03 (q, J = 3.0 Hz), 125.66, 124.68 (q, J = 270 Hz); MS (ESI) m/z: 410 [M+H]$^{+}$.

CY-09
^{1}H NMR (600 MHz, DMSO-d_6) δ 8.07 (d, J = 12.0 Hz, 2H), 7.91 (s, 1H), 7.77 (d, J = 12 Hz, 2H), 7.74 (s, 1H), 7.67 (d, J = 12 Hz, 1H), 7.62–7.57 (m, 2H), 5.33 (s, 2H); ^{13}C NMR (150 MHz, DMSO-d_6) δ 193.62, 167.07, 166.69, 136.70, 136.26, 132.66, 132.12, 131.77, 130.71, 130.22, 129.82, 129.28 (q, J = 31.5 Hz), 124.68 (q, J = 4.5 Hz), 124.61 (q, J = 4.5 Hz), 124.10 (q, J = 270 Hz), 54.93, 46.87; MS (ESI) m/z: 424 [M+H]$^{+}$.

Biotin–CY-09
^{1}H NMR (600 MHz, DMSO-d_6) δ 7.92 (s, 1H), 7.79–7.71 (m, 4H), 7.71–7.66 (m, 1H), 7.66–7.57 (m, 4H), 6.42 (s, 1H), 6.36 (s, 1H), 5.35 (s, 2H), 4.34–4.28 (m, 1H), 4.16–4.10 (m, 1H), 3.69–3.45 (m, 8H), 3.13–3.06 (m, 1H), 3.06–2.97 (m, 2H), 2.82 (dd, J = 12.4, 5.1 Hz, 1H), 2.58 (d, J = 12.4 Hz, 1H), 2.39–2.25 (m, 2H), 2.04 (t, J = 7.4 Hz, 2H), 1.65–1.58 (m, 1H), 1.55–1.44 (m, 5H), 1.42–1.35 (m, 2H), 1.33–1.22 (m, 4H); ^{13}C NMR (150 MHz, DMSO-d_6) δ 194.0, 172.3, 171.3, 168.7, 167.5, 163.1, 138.1, 136.7, 134.4, 133.0, 132.2, 131.2, 130.2, 129.7 (q, J = 31.7 Hz), 128.6, 125.1 (q, J = 3.6 Hz), 125.0 (q, J = 3.7 Hz), 124.5 (q, J = 270.7 Hz), 124.0, 61.5, 59.7, 55.9, 47.3, 38.7, 35.7, 32.7, 29.5, 28.7, 28.5, 26.6, 25.8, 24.9; MS (ESI) m/z: 832 [M+H]$^{+}$.

Reagents
MSU, nigericin, ATP, PMA, BHB, DL-sulforaphane, poly(dA:dT), and glucose were purchased from Sigma-Aldrich. MCC950 was acquired from Selleck. BAY 11-7082, isoliquiritigenin, parthenolide, flufenamic acid, and mefenamic acid were acquired from Topscience. Human recombinant insulin was bought from Novo Nordisk. The One Touch Ultra Blood Glucose Test System kit was bought from Roche. Ultrapure LPS, Pam3CSK4, MitoTracker, and MitoSOX were obtained from Invitrogen. Protein G agarose and streptavi-din–coated beads were respectively supplied by Millipore and Pierce Biochemicals. ATP-coupled beads were from Bio-World Company. Anti-mouse caspase-1 (p20; AG-20B-0042) and anti-NLRP3 (AG-20B-0014) were from Adipogen. Anti-ASC (sc-22514-R) and anti-NEK7 (SC-50756) were from Santa Cruz. Anti-β-actin (P30002) was bought from Abmart. Anti-human caspase-1 was from Cell Signaling Technology. Anti-human cleaved IL-1β (A5208206) was from Sangon Biotech. Anti-mouse IL-1β (p17; AF-401-NA) was from R&D Systems. Anti-Flag (F2555) and anti-Mcherry (V4888) were from Sigma-Aldrich. Recombinant human NLRP3 was from Novus Biologicals. A standard HFD (D12492, 60% kcal fat) was from Research Diet Company.

Human samples
Adult peripheral blood samples were obtained from healthy donors at Hefei Blood Bank, and the experimental protocol was performed according to the approved guidelines established by the Institutional Human Research Subjects Protection Committee of the Ethics Committee of the University of Science and Technology of China. Synovial fluid was obtained from five patients with gout with serum uric acid levels >500 µmol/l and knee effusion. To use these clinical materials for research purposes, prior patient written informed consent and approval from the Institutional Research Ethics Committee of Anhui Provincial Hospital were obtained (approval no. 20160167).

Protein expression and purification
To produce purified recombinant proteins, HEK-293T cells were transiently transfected with plasmids encoding Flag-tagged NLRP3, NLRP3 Walker A mutant, NLRP3 Walker B mutant, NOD2, NLRC4, RIG-1, and NLRP1. 48 h after transfection, the cells were washed twice in cold PBS and collected by lysing cells in a buffer containing 50 mM Hepes, 150 mM NaCl, and 0.4% CHAPS. The insoluble fraction was removed by centrifugation at 14,000 rpm for 15 min at 4°C. Supernatants were incubated with Flag-M2 monoclonal antibody–agarose for 2.5 h at 4°C on rotation and then washed with wash buffer A (50 mM Hepes, pH 7.4, 150 mM NaCl, 2 mM DTT, 2 mM ATP, and 0.1% CHAPS) twice and another two times with wash buffer B (50 mM Hepes, pH 7.4, 200 mM NaCl, and 0.1% CHAPS). For elution of Flag-tagged proteins, beads were incubated in elution buffer (50 mM Hepes, pH 7.4, 500 mM NaCl, 0.1% CHAPS, and 100 mg/ml Flag peptide) for 90 min at 4°C on rotation. Eluted fractions were pooled and concentrated by centrifugation before ultrafiltration device (UFC910024; Merck Millipore) to remove proteins <100 kD. To further purify the Flag-tagged proteins, they were subjected to second round of Flag-M2 monoclonal antibody–agarose binding and Flag peptide elution.

For producing purified GFP-NLRP3 protein, His-GFP-NLRP3 plasmid was transiently transfected into HEK-293T cells. After 48 h, the cells were collected and lysed in

lysis buffer (50 mM Hepes, pH 7.4, 150 mM NaCl, and 0.4% CHAPS) for 30 min. After sonication, the insoluble fraction was removed by centrifugation at 14,000 rpm for 15 min at 4°C. The His–GFP–NLRP3 protein was initially purified by incubation with nickel–nitrilotriacetic acid matrices (QIA GEN) for 45 min at room temperature. Histidine pull-down products were eluted in elution buffer after washing twice with lysis buffer. The eluted fractions were filtered through a 0.45-μm syringe filter and concentrated by the ultrafiltration device (Merck Millipore) to remove proteins <10 kD. Afterward, 5,000 μl of the final eluted fractions was injected into a Superdex 200 10/300 GLcolumn (GE Healthcare). Protein was further purified in 50 mM Hepes, pH 7.4, and 150 mM NaCl on an AKTA purifier (GE Healthcare). Each tube of fraction (10 μl each) was resolved by SDS-PAGE gels and detected by anti-His antibody. Solution in the tubes containing His–GFP–NLRP3 protein was collected together and subjected to concentration by ultrafiltration device (UFC910024; Merck Millipore) to remove proteins <100 kD.

MST assay

The K_D value was measured using the Monolith NT.115 instrument (NanoTemper Technologies). A range of concentrations of CY-09 (from 0.025 mM to 1.2 nM) were incubated with 200 nM of purified His–GFP–NLRP3 protein for 40 min in assay buffer (50 mM Hepes, 10 mM MgCl$_2$, 100 mM NaCl, pH 7.5, and 0.05% Tween 20). The samples were loaded into the NanoTemper glass capillaries, and MST was performed using 100% LED power and 80% MST power. The K_D value was calculated using the mass action equation via the NanoTemper software from duplicate reads of an experiment.

Microsomal stability

Microsomal stability was determined in Crown Bioscience CY-09 or control compound DMSO stock solution (10 mM) diluted with 50% methanol to a concentration of 100 μM. 6 μl of 100 μM compound solution was combined with 534 μl of liver microsome solution (0.7 mg protein/ml potassium phosphate buffer) to produce the compound working solution. A 90-μl aliquot of this working solution was incubated at 37°C for 10 min before the addition of NADPH regenerating system (10 μl) to start the reaction. Reactions were stopped at 0, 10, 30, and 60 min by addition of 300 μl cold acetonitrile (containing tolbutamide as internal standard at 500 nM) and centrifuged at 4,000 rpm for 20 min. The supernatant (100 μl) was added to water (300 μl) and analyzed by liquid chromatography/tandem mass spectrometry. The ratio of peak area of test compound remaining/internal standard was used to determine reduction in concentration of test compound over time. The $t_{1/2}$ and hepatic clearance (CL^{hep}) were then calculated.

Determination of the pharmacokinetic properties of CY-09 in mice

The pharmacokinetics of CY-09 were determined after single i.v. and oral administration in C57BL/6J mice ($n = 3$ at each time point) at doses of 5 and 10 mg/kg, respectively. Blood samples were collected at 0.08, 0.25, 0.5, 1, 2, 4, 8, 10, and 24 h (i.v.) and 0.25, 0.5, 1, 2, 4, 8, 10, and 24 h (oral) after administration. Then the samples were quantified by liquid chromatography/tandem mass spectrometry, and data analysis was conducted using WinNonlin v.6.3.

Cell preparation and stimulation

Human THP-1 cells were cultured in RPMI 1640 medium, supplemented with 10% FBS and 50 μM 2-mercaptoethanol. Differentiated THP-1 cells were acquired by coculturing with 100 nM PMA for 3 h. Human PBMCs were isolated using Ficoll–Paque. BMDMs were collected from mice tibia and femoral bone marrow as described elsewhere (Yan et al., 2015) and cultured in DMEM complemented with 10% FBS, 1 mM sodium pyruvate, and 2 mM L-glutamine in the presence of 15% L929 culture supernatants. HEK-293T cells were cultured in DMEM supplemented with 10% FBS. THP-1, L929, and HEK-293T cells were from ATCC and were routinely tested for mycoplasma contamination. Human PBMCs were isolated from freshly drawn peripheral venous blood with Human Lymphocyte Separation Medium (catalog no. P8610-200; Solarbio) according to the manufacturer's instructions. PBMCs were cultured overnight before stimulation in RPMI 1640 medium containing 10% FBS and antibiotics. The fresh isolated SFCs were centrifuged and washed with PBS three times and then incubated with RPMI 1640 medium containing 1% FBS for 20 h.

To induce NLRP3 inflammasome activation, 5×10^5/ml BMDMs and 6×10^6/ml PBMCs were plated in 12-well plates. The following morning, the medium was replaced, and cells were stimulated with 50 ng/ml LPS or 400 ng/ml Pam3CSK4 (for noncanonical inflammasome activation) for 3 h. After that, CY-09 or other inhibitors were added into the culture for another 30 min, and then the cells were stimulated for 4 h with MSU (150 μg/ml), *Salmonella typhimurium* (multiplicity of infection) or for 30 min with ATP (2.5 mM) or nigericin (10 μM). Cells were transfected with poly(dA:dT) (0.5 μg/ml) for 4 h or LPS (500 ng/ml) overnight using Lipofectamine 2000 (Invitrogen). Cell extracts and precipitated supernatants were analyzed by immunoblot.

Confocal microscopy

Confocal analysis was performed as previously described (Yan et al., 2015). In brief, 2×10^5/ml BMDMs were plated on coverslips (Thermo Fisher Scientific). On the following day, the medium was replaced with Opti-MEM (1% FBS) containing LPS (50 ng/ml) for 3 h, and then the indicated doses of CY-09 were added for another 30 min. BMDMs were then used for stimulation and staining with MitoTracker Red (50 nM) or MitoSOX (5 μM). After three times washing with ice-cold PBS, the cells were fixed with 4% PFA in PBS for 15 min at room temperature and then washed with PBS with Tween 20 three times. Confocal microscopic analyses were performed using a Zeiss LSM700.

ELISA

Supernatants from cell culture, tissue culture, or serum were assayed for mouse IL-1β, IL-6, TNF-α, MCP-1, and human IL-1β or TNF-α (R&D Systems) according to the manufacturer's instructions. Fasted plasma insulin level was detected by using a mouse insulin ELISA kit supplied by Crystal Chemical (catalog no. 90080).

MSU–induced peritonitis

C57BL/6J mice were injected i.p. with 40 mg/kg CY-09 or vehicle 30 min before i.p. injection of MSU (1 mg MSU crystals dissolved in 0.5 ml sterile PBS). After 6 h, mice were killed, and peritoneal cavities underwent lavage with 10 ml ice-cold PBS. Peritoneal lavage fluid was assessed by flow cytometry with the neutrophil markers Ly6G and CD11b for analysis of the recruitment of polymorph nuclear neutrophils. IL-1β production in serum or peritoneal lavage fluid was determined using ELISA.

Intracellular potassium or chloride detection

For accurate measurement of intracellular potassium, BMDMs were plated overnight in 6-well plates and then primed with 50 ng/ml LPS for 3 h. After that, cells were treated with CY-09 for 30 min and then stimulated with nigericin for 30 min. Culture medium was thoroughly aspirated and lysed with 65% ultrapure HNO_3. Intracellular K^+ measurements were performed by inductively coupled plasma optical emission spectrometry with a PerkinElmer Optima 2000 DV spectrometer using yttrium as the internal standard.

For accurate measurement of the intracellular chloride, BMDMs were plated overnight in 12-well plates and then primed with 50 ng/ml LPS for 3 h. After that, cells were treated with CY-09 or MCC950 for 30 min and then stimulated with nigericin for 15 min. The supernatants of 12-well plates were removed, ddH2O was added (200 µl/well), and the supernatants were kept 15 min at 37°C. The lysates were transferred to 1.5-ml EP tube, and centrifuged at 10,000 g for 5 min. 160-µl supernatants were then transferred to a new 1.5-ml EP tube and mixed with 40 µl MQAE (10 µM). Absorbance was tested using BioTek Multi-Mode Microplate Readers (Synergy2). A control was settled in every experiment to determine the extracellular amount of chloride remaining after aspiration, and this value was subtracted.

Immunoprecipitation (IP) and pulldown assay

For the endogenous IP assay, BMDMs were stimulated and lysed with NP-40 lysis buffer with complete protease inhibitor. The cell lysates were incubated overnight at 4°C with the primary antibodies and Protein G Mag Sepharose (GE Healthcare). The proteins bound by antibody were precipitated by protein G beads and subjected to immunoblotting analysis. For the exogenous IP assay, HEK-293T cells (3 × 10^5/ml) were transfected with plasmids in 6-well plates via polyethylenimine. After 24 h, cells were collected and lysed with NP-40 lysis buffer. Protein extracts were immunoprecipitated with anti-Flag antibody–coated beads and then assessed by immunoblot analysis.

For pull-down assay, BMDMs or 293T lysates were collected and centrifuged at 8,000 rpm. The supernatant was transferred to another tube and the cell debris thoroughly discarded. Prewashed streptavidin beads were added into the supernatant, allowing 2 h preincubation with motion at 4°C and centrifuging at 8,000 rpm. The supernatant was transferred to another tube, and the streptavidin beads were discarded to remove unspecific binding proteins. The pretreated supernatant and purified human recombinant NLRP3 proteins (dissolving in the lysis buffer) were incubated with indicated doses of free CY-09, followed by incubation with indicated doses of biotin–CY-09 for 1 h. After that, the samples were then incubated with prewashed streptavidin beads overnight. Beads were respectively washed twice with 0.1% Tween 20 in PBS and 1% NP-40 in PBS to remove unspecific binding proteins and boiled in SDS buffer.

NLRP3 ATPase activity and ATP binding assay

For ATPase activity assay, purified recombinant human proteins (1.4 ng/µl) were incubated at 37°C with indicated concentrations of CY-09 for 15 min in the reaction buffer. ATP (25 µm, Ultra-Pure ATP) was then added, and the mixture was further incubated at 37°C for another 40 min. The amount of ATP converted into adenosine diphosphate (ADP) was determined by luminescent ADP detection with ADP-Glo Kinase Assay kit (Promega, Madison, MI, USA) according to the manufacturer's protocol. The results were expressed as percentage of residual enzyme activity to the vehicle-treated enzyme.

For ATP binding assay, purified NLRP3 protein (0.1 ng/µl) were incubated with ATP binding agarose for 1 h and then different concentrations of CY-09 was added and incubated for 2 h with motion at 4°C. Beads were washed and boiled in loading buffer. Samples were subjected to immunoblotting analysis.

ASC oligomerization assay

BMDMs were seeded at 1×10^6/ml in 6-well plates. The following day, the medium was replaced, and cells were primed with 50 ng/ml LPS for 3 h. The cells were treated with CY-09 for 30 min and then stimulated with nigericin for 30 min. The supernatants were removed, cells were rinsed in ice-cold PBS, and then cells were lysed by NP-40 for 30 min. Lysates were centrifuged at 330 g for 10 min at 4°C. The pellets were washed twice in 1 ml ice-cold PBS and resuspended in 500 µl PBS. 2 mM disuccinimydyl suberate was added to the resuspended pellets, which were incubated at room temperature for 30 min with rotation. Samples were then centrifuged at 330 g for 10 min at 4°C. The cross-linked pellets were resuspended in 30 µl sample buffer and then boiled and analyzed by immunoblotting.

SDD–AGE

The oligomerization of NLRP3 was analyzed according to a published protocol (Hou et al., 2011). Cells were lysed with

Triton X-100 lysis buffer (0.5% Triton X-100, 50 mM Tris-Hcl, 150 mM NaCL, 10% glycerol, 1 mM PMSF, and protease inhibitor cocktail), which were then resuspended in 1× sample buffer (0.5× TBE, 10% glycerol, 2% SDS, and 0.0025% bromophenol blue) and loaded onto a vertical 1.5% agarose gel. After electrophoresis in the running buffer (1× TBE and 0.1% SDS) for 1 h with a constant voltage of 80 V at 4°C, the proteins were transferred to Immobilon membrane (Millipore) for immunoblotting. 1× TBE buffer contains 89 mM Tris, pH 8.3, 89 mM boric acid, and 2 mM EDTA.

Human NLRP3 homology modeling and docking calculation

The human NLRP3 model was prepared by ModWeb Server, which uses the MODELLER program in homology modeling. One chain from crystal structure of rabbit NOD2 bound with ADP (Protein Data Bank accession no. 5IRM) was used as template structure. Small-molecule docking was done by AutoDock with AutoDockTools. The search space was set near the ADP-binding site of rabbit NOD2, and the Lamarckian genetic algorithm was used. The model was defined as rigid, while the ligand was flexible. The model with the best conformation of ligand was further optimized by molecular dynamics simulation using Gromacs. After that, docking was repeated once again. Molecular graphics was prepared by PyMOL.

MWS mouse model

$Nlrp3^{A350VneoR}$ mice were crossed with LysM-Cre mice (B6.129P2-$Lyz2^{tm1(cre)Ifo}$/J). CY-09 (20 mg/kg) or MCC950 (20 mg/kg) were administered orally every day starting at day 4 after birth. The weight and survival of mice were monitored every day.

HFD and CY-09 treatment

WT or $Nlrp3^{-/-}$ mice at the age of 6 wk, with similar plasma glucose levels and body weights were randomized into different groups. For generation of HFD-induced diabetic mice, mice were fed with HFD for 14 wk. The diabetic mice were treated with CY-09 (i.p.) at a dose of 2.5 mg/kg once a day for 6 wk. The mice were maintained with HFD when used for CY-09 treatment and the subsequent experiments.

Blood glucose assay

Glucose levels in blood collected from the tail vein were determined using a OneTouch Ultra Blood Glucose Test System kit (Roche).

Glucose tolerance and insulin tolerance tests

Glucose tolerance tests were performed via i.p. injection of glucose at 1.5 g/kg after 14 h fasting from the beginning of dark cycle. Insulin tolerance tests were performed via i.p. injection of human recombinant insulin (Novo Nordisk) at a dose of 0.75 U/kg after 4 h fasting. Blood glucose levels were measured from the tail veil at 0, 15, 30, 60, 90, and 120 min after glucose or insulin injection.

Cytochrome P450 inhibition

Cytochrome P450 inhibitory effects of CY-09 against five major CYP isozymes (1A2, 2C9, 2C19, 2D6, and 3A4) were determined at Wuxi AppTech. A working stock solution of CY-09 (10 mM in DMSO) was diluted using phosphate buffer to a concentration of 100 µM. Five inhibitor stock solutions were prepared at a concentration of 3 mM in DMSO: α-naphthoflavone, sulfaphenazole, N-3-benzylnirvanol, quinidine, and ketoconazole. The inhibitor stocks were diluted using phosphate buffer to a concentration of 30 µM. A cocktail of substrates (phenacetin, diclofenac, S-mephenytoin, dextromethorphan, and midazolam) for five major CYP isozymes (1A2, 2C9, 2C19, 2D6, and 3A4) was prepared by dilution of methanol stock solutions using phosphate buffer. CY-09, known inhibitor, or blank solution (20 µl of working stock solution) and substrate cocktail solution (20 µl) were incubated at 37°C with human liver microsomes (158 µl 0.253 mg/ml in phosphate buffer) for 10 min before addition of the cofactor NADPH (20 µl 10 mM solution in 33 mM MgCl₂). Incubation was continued, and aliquots were removed at 0, 5, 10, 20, 30, and 60 min and then mixed with cold acetonitrile (containing tolbutamide as internal MS standard at 200 ng/ml) and centrifuged at 4,000 rpm for 20 min. The supernatant was analyzed by liquid chromatography/tandem mass spectrometry to determine the peak area of metabolite and internal standard. Peak areas determined in the presence and absence of test compound were used to determine percentage inhibition. SigmaPlot v.11 was used to plot percentage control activity versus the test compound concentrations and for nonlinear regression analysis of the data. IC_{50} values were determined using a three-parameter logistic equation. IC_{50} values were reported as ">50 µM" when percentage inhibition at the highest concentration (50 µM) was <50%.

hERG channel assay

The manual patch-clamp method (QPatch^{HTX}) was used at WuXiAppTech to evaluate the effects of CY-09 on the hERG potassium channel. CHO cells that stably express hERG potassium channels from Aviva Biosciences were used. The inhibition of CY-09 and amitriptyline as positive control on whole-cell hERG currents were determined.

Histological analysis

Mouse tissues were postfixed in 4% PFA for 24 h at 4°C and sectioned after embedding in paraffin. The sections were prepared and stained with H&E using standard procedures. Slides were examined under a Nikon ECLIPSE Ci biological microscope, and images were captured with a Nikon DS-U3 color digital camera.

Statistical analyses

All values are expressed as the mean and SEM. Statistical analysis was performed using the unpaired t test for two groups or two-way ANOVA (GraphPad Software) using for multiple groups with all data points showing a normal distribution. No

exclusion of data points was used. The researchers were not blinded to the distribution of treatment groups when performing experiments and data assessment. Sample sizes were selected on the basis of preliminary results to ensure an adequate power. P-values < 0.05 were considered to indicate statistical significance.

Online supplemental material

Fig. S1 includes additional data related to Fig. 2, indicating that CY-09 has no effect on LPS-induced priming in BMDMs and blocks nigericin-induced BMDM death. Fig. S2 includes additional data related to Fig. 3, showing that apart from CY-09 and MCC950, the other inhibitors have broad anti-inflammatory activity. Fig. S3 includes additional data related to Fig. 5, indicating that CY-09 directly binds to NLRP3. Fig. S4 includes additional data related to Fig. 9, showing that CY-09 had no effect on the metabolic parameters and serum chemistry of normal lean mice. Fig. S5 includes additional data related to Fig. 10, indicating that CY-09 can suppress the preactivated NLRP3 inflammasome in SFCs from four patients with arthritis. Table S1 shows the microsomal stability of CY-09. Table S2 indicates the effect of CY-09 on CYP. Table S3 shows the effect of CY-09 on the hERG channel. Table S4 indicates the pharmacokinetic properties of CY-09 in mice.

REFERENCES

Alberti, S., R. Halfmann, O. King, A. Kapila, and S. Lindquist. 2009. A systematic survey identifies prions and illuminates sequence features of prionogenic proteins. *Cell*. 137:146–158. https://doi.org/10.1016/j.cell.2009.02.044

Broderick, L., D. De Nardo, B.S. Franklin, H.M. Hoffman, and E. Latz. 2015. The inflammasomes and autoinflammatory syndromes. *Annu. Rev. Pathol.* 10:395–424. https://doi.org/10.1146/annurev-pathol-012414-040431

Brydges, S.D., J.L. Mueller, M.D. McGeough, C.A. Pena, A. Misaghi, C. Gandhi, C.D. Putnam, D.L. Boyle, G.S. Firestein, A.A. Horner, et al. 2009. Inflammasome-mediated disease animal models reveal roles for innate but not adaptive immunity. *Immunity*. 30:875–887. https://doi.org/10.1016/j.immuni.2009.05.005

Chen, G., M.H. Shaw, Y.G. Kim, and G. Nuñez. 2009. NOD-like receptors: role in innate immunity and inflammatory disease. *Annu. Rev. Pathol.* 4:365–398. https://doi.org/10.1146/annurev.pathol.4.110807.092239

Cocco, M., C. Pellegrini, H. Martinez-Banaclocha, M. Giorgis, E. Marini, A. Costale, G. Miglio, M. Fornai, L. Antonioli, G. Lopez-Castejon, et al. 2017. Development of an acrylate derivative targeting the NLRP3 inflammasome for the treatment of inflammatory bowel disease. *J. Med. Chem.* 60:3656–3671. https://doi.org/10.1021/acs.jmedchem.6b01624

Coll, R.C., A.A. Robertson, J.J. Chae, S.C. Higgins, R. Muñoz-Planillo, M.C. Inserra, I. Vetter, L.S. Dungan, B.G. Monks, A. Stutz, et al. 2015. A small-molecule inhibitor of the NLRP3 inflammasome for the treatment of inflammatory diseases. *Nat. Med.* 21:248–255. https://doi.org/10.1038/nm.3806

Daniels, M.J., J. Rivers-Auty, T. Schilling, N.G. Spencer, W. Watremez, V. Fasolino, S.J. Booth, C.S. White, A.G. Baldwin, S. Freeman, et al. 2016. Fenamate NSAIDs inhibit the NLRP3 inflammasome and protect against Alzheimer's disease in rodent models. *Nat. Commun.* 7:12504. https://doi.org/10.1038/ncomms12504

Davis, B.K., H. Wen, and J.P. Ting. 2011. The inflammasome NLRs in immunity, inflammation, and associated diseases. *Annu. Rev. Immunol.* 29:707–735. https://doi.org/10.1146/annurev-immunol-031210-101405

Dempsey, C., A. Rubio Araiz, K.J. Bryson, O. Finucane, C. Larkin, E.L. Mills, A.A.B. Robertson, M.A. Cooper, L.A.J. O'Neill, and M.A. Lynch. 2017. Inhibiting the NLRP3 inflammasome with MCC950 promotes non-phlogistic clearance of amyloid-β and cognitive function in APP/PS1 mice. *Brain Behav. Immun.* 61:306–316. https://doi.org/10.1016/j.bbi.2016.12.014

Dick, M.S., L. Sborgi, S. Rühl, S. Hiller, and P. Broz. 2016. ASC filament formation serves as a signal amplification mechanism for inflammasomes. *Nat. Commun.* 7:11929. https://doi.org/10.1038/ncomms11929

Dinarello, C.A., and J.W. van der Meer. 2013. Treating inflammation by blocking interleukin-1 in humans. *Semin. Immunol.* 25:469–484. https://doi.org/10.1016/j.smim.2013.10.008

Dinarello, C.A., A. Simon, and J.W. van der Meer. 2012. Treating inflammation by blocking interleukin-1 in a broad spectrum of diseases. *Nat. Rev. Drug Discov.* 11:633–652. https://doi.org/10.1038/nrd3800

Duewell, P., H. Kono, K.J. Rayner, C.M. Sirois, G. Vladimer, F.G. Bauernfeind, G.S. Abela, L. Franchi, G. Nuñez, M. Schnurr, et al. 2010. NLRP3 inflammasomes are required for atherogenesis and activated by cholesterol crystals. *Nature*. 464:1357–1361. https://doi.org/10.1038/nature08938

Duncan, J.A., D.T. Bergstralh, Y. Wang, S.B. Willingham, Z. Ye, A.G. Zimmermann, and J.P. Ting. 2007. Cryopyrin/NALP3 binds ATP/dATP, is an ATPase, and requires ATP binding to mediate inflammatory signaling. *Proc. Natl. Acad. Sci. USA*. 104:8041–8046. https://doi.org/10.1073/pnas.0611496104

Fautrel, B. 2012. Economic benefits of optimizing anchor therapy for rheumatoid arthritis. *Rheumatology (Oxford)*. 51(Suppl 4):iv21–iv26. https://doi.org/10.1093/rheumatology/kes088

Fu, S.P., J.F. Wang, W.J. Xue, H.M. Liu, B.R. Liu, Y.L. Zeng, S.N. Li, B.X. Huang, Q.K. Lv, W. Wang, and J.X. Liu. 2015. Anti-inflammatory effects of BHBA in both in vivo and in vitro Parkinson's disease models are mediated by GPR109A-dependent mechanisms. *J. Neuroinflammation*. 12:9. https://doi.org/10.1186/s12974-014-0230-3

Goldberg, E.L., J.L. Asher, R.D. Molony, A.C. Shaw, C.J. Zeiss, C. Wang, L.A. Morozova-Roche, R.I. Herzog, A. Iwasaki, and V.D. Dixit. 2017. β-Hydroxybutyrate deactivates neutrophil NLRP3 inflammasome to relieve gout flares. *Cell Reports*. 18:2077–2087. https://doi.org/10.1016/j.celrep.2017.02.004

Greaney, A.J., N.K. Maier, S.H. Leppla, and M. Moayeri. 2016. Sulforaphane inhibits multiple inflammasomes through an Nrf2-independent mechanism. *J. Leukoc. Biol.* 99:189–199. https://doi.org/10.1189/jlb.3A0415-155RR

He, Y., S. Varadarajan, R. Muñoz-Planillo, A. Burberry, Y. Nakamura, and G. Núñez. 2014. 3,4-Methylenedioxy-β-nitrostyrene inhibits NLRP3 inflammasome activation by blocking assembly of the inflammasome. *J. Biol. Chem.* 289:1142–1150. https://doi.org/10.1074/jbc.M113.515080

He, Y., M.Y. Zeng, D. Yang, B. Motro, and G. Núñez. 2016. NEK7 is an essential mediator of NLRP3 activation downstream of potassium efflux. *Nature.* 530:354–357. https://doi.org/10.1038/nature16959

Heiss, E., C. Herhaus, K. Klimo, H. Bartsch, and C. Gerhäuser. 2001. Nuclear factor kappa B is a molecular target for sulforaphane-mediated anti-inflammatory mechanisms. *J. Biol. Chem.* 276:32008–32015. https://doi.org/10.1074/jbc.M104794200

Heneka, M.T., M.P. Kummer, A. Stutz, A. Delekate, S. Schwartz, A. Vieira-Saecker, A. Griep, D. Axt, A. Remus, T.C. Tzeng, et al. 2012. NLRP3 is activated in Alzheimer's disease and contributes to pathology in APP/PS1 mice. *Nature.* 493:674–678. https://doi.org/10.1038/nature11729

Honda, H., Y. Nagai, T. Matsunaga, S. Saitoh, S. Akashi-Takamura, H. Hayashi, I. Fujii, K. Miyake, A. Muraguchi, and K. Takatsu. 2012. Glycyrrhizin and isoliquiritigenin suppress the LPS sensor toll-like receptor 4/MD-2 complex signaling in a different manner. *J. Leukoc. Biol.* 91:967–976. https://doi.org/10.1189/jlb.0112038

Honda, H., Y. Nagai, T. Matsunaga, N. Okamoto, Y. Watanabe, K. Tsuneyama, H. Hayashi, I. Fujii, M. Ikutani, Y. Hirai, et al. 2014. Isoliquiritigenin is a potent inhibitor of NLRP3 inflammasome activation and diet-induced adipose tissue inflammation. *J. Leukoc. Biol.* 96:1087–1100. https://doi.org/10.1189/jlb.3A0114-005RR

Hou, F., L. Sun, H. Zheng, B. Skaug, Q.X. Jiang, and Z.J. Chen. 2011. MAVS forms functional prion-like aggregates to activate and propagate antiviral innate immune response. *Cell.* 146:448–461. https://doi.org/10.1016/j.cell.2011.06.041

Jesus, A.A., and R. Goldbach-Mansky. 2014. IL-1 blockade in autoinflammatory syndromes. *Annu. Rev. Med.* 65:223–244. https://doi.org/10.1146/annurev-med-061512-150641

Jo, E.K., J.K. Kim, D.M. Shin, and C. Sasakawa. 2016. Molecular mechanisms regulating NLRP3 inflammasome activation. *Cell. Mol. Immunol.* 13:148–159. https://doi.org/10.1038/cmi.2015.95

Juliana, C., T. Fernandes-Alnemri, J. Wu, P. Datta, L. Solorzano, J.W. Yu, R. Meng, A.A. Quong, E. Latz, C.P. Scott, and E.S. Alnemri. 2010. Anti-inflammatory compounds parthenolide and BAY 11-7082 are direct inhibitors of the inflammasome. *J. Biol. Chem.* 285:9792–9802. https://doi.org/10.1074/jbc.M109.082305

Juliana, C., T. Fernandes-Alnemri, S. Kang, A. Farias, F. Qin, and E.S. Alnemri. 2012. Non-transcriptional priming and deubiquitination regulate NLRP3 inflammasome activation. *J. Biol. Chem.* 287:36617–36622. https://doi.org/10.1074/jbc.M112.407130

Lamkanfi, M., and V.M. Dixit. 2012. Inflammasomes and their roles in health and disease. *Annu. Rev. Cell Dev. Biol.* 28:137–161. https://doi.org/10.1146/annurev-cellbio-101011-155745

Liu, J., and X. Cao. 2016. Cellular and molecular regulation of innate inflammatory responses. *Cell. Mol. Immunol.* 13:711–721. https://doi.org/10.1038/cmi.2016.58

Lu, A., V.G. Magupalli, J. Ruan, Q. Yin, M.K. Atianand, M.R. Vos, G.F. Schröder, K.A. Fitzgerald, H. Wu, and E.H. Egelman. 2014. Unified polymerization mechanism for the assembly of ASC-dependent inflammasomes. *Cell.* 156:1193–1206. https://doi.org/10.1016/j.cell.2014.02.008

Lu, B., T. Nakamura, K. Inouye, J. Li, Y. Tang, P. Lundbäck, S.I. Valdes-Ferrer, P.S. Olofsson, T. Kalb, J. Roth, et al. 2012. Novel role of PKR in inflammasome activation and HMGB1 release. *Nature.* 488:670–674. https://doi.org/10.1038/nature11290

Ma, T., J.R. Thiagarajah, H. Yang, N.D. Sonawane, C. Folli, L.J. Galietta, and A.S. Verkman. 2002. Thiazolidinone CFTR inhibitor identified by high-throughput screening blocks cholera toxin-induced intestinal fluid secretion. *J. Clin. Invest.* 110:1651–1658. https://doi.org/10.1172/JCI0216112

MacDonald, J.A., C.P. Wijekoon, K.C. Liao, and D.A. Muruve. 2013. Biochemical and structural aspects of the ATP-binding domain in inflammasome-forming human NLRP proteins. *IUBMB Life.* 65:851–862. https://doi.org/10.1002/iub.1210

Martinon, F., V. Pétrilli, A. Mayor, A. Tardivel, and J. Tschopp. 2006. Gout-associated uric acid crystals activate the NALP3 inflammasome. *Nature.* 440:237–241. https://doi.org/10.1038/nature04516

Martinon, F., A. Mayor, and J. Tschopp. 2009. The inflammasomes: guardians of the body. *Annu. Rev. Immunol.* 27:229–265. https://doi.org/10.1146/annurev.immunol.021908.132715

Masters, S.L., A. Dunne, S.L. Subramanian, R.L. Hull, G.M. Tannahill, F.A. Sharp, C. Becker, L. Franchi, E. Yoshihara, Z. Chen, et al. 2010. Activation of the NLRP3 inflammasome by islet amyloid polypeptide provides a mechanism for enhanced IL-1β in type 2 diabetes. *Nat. Immunol.* 11:897–904. https://doi.org/10.1038/ni.1935

McGonagle, D., A.L. Tan, S. Shankaranarayana, J. Madden, P. Emery, and M.F. McDermott. 2007. Management of treatment resistant inflammation of acute on chronic tophaceous gout with anakinra. *Ann. Rheum. Dis.* 66:1683–1684. https://doi.org/10.1136/ard.2007.073759

McQueen, F.M., A. Chhana, and N. Dalbeth. 2012. Mechanisms of joint damage in gout: evidence from cellular and imaging studies. *Nat. Rev. Rheumatol.* 8:173–181. https://doi.org/10.1038/nrrheum.2011.207

Muñoz-Planillo, R., P. Kuffa, G. Martínez-Colón, B.L. Smith, T.M. Rajendiran, and G. Núñez. 2013. K^+ efflux is the common trigger of NLRP3 inflammasome activation by bacterial toxins and particulate matter. *Immunity.* 38:1142–1153. https://doi.org/10.1016/j.immuni.2013.05.016

Nathan, D.M., J.B. Buse, M.B. Davidson, E. Ferrannini, R.R. Holman, R. Sherwin, and B. Zinman; American Diabetes Association; European Association for Study of Diabetes. 2009. Medical management of hyperglycemia in type 2 diabetes: a consensus algorithm for the initiation and adjustment of therapy: a consensus statement of the American Diabetes Association and the European Association for the Study of Diabetes. *Diabetes Care.* 32:193–203. https://doi.org/10.2337/dc08-9025

Netea, M.G., F.L. van de Veerdonk, J.W. van der Meer, C.A. Dinarello, and L.A. Joosten. 2015. Inflammasome-independent regulation of IL-1-family cytokines. *Annu. Rev. Immunol.* 33:49–77. https://doi.org/10.1146/annurev-immunol-032414-112306

Nowarski, R., R. Jackson, N. Gagliani, M.R. de Zoete, N.W. Palm, W. Bailis, J.S. Low, C.C. Harman, M. Graham, E. Elinav, and R.A. Flavell. 2015. Epithelial IL-18 equilibrium controls barrier function in colitis. *Cell.* 163:1444–1456. https://doi.org/10.1016/j.cell.2015.10.072

Pétrilli, V., S. Papin, C. Dostert, A. Mayor, F. Martinon, and J. Tschopp. 2007. Activation of the NALP3 inflammasome is triggered by low intracellular potassium concentration. *Cell Death Differ.* 14:1583–1589. https://doi.org/10.1038/sj.cdd.4402195

Pongkorpsakol, P., S. Satitsri, P. Wongkrasant, P. Chittavanich, S. Kittayaruksakul, P. Srimanote, V. Chatsudthipong, and C. Muanprasat. 2017. Flufenamic acid protects against intestinal fluid secretion and barrier leakage in a mouse model of *Vibrio cholerae* infection through NF-κB inhibition and AMPK activation. *Eur. J. Pharmacol.* 798:94–104. https://doi.org/10.1016/j.ejphar.2017.01.026

Qaseem, A., L.L. Humphrey, D.E. Sweet, M. Starkey, and P. Shekelle. Clinical Guidelines Committee of the American College of Physicians. 2012. Oral pharmacologic treatment of type 2 diabetes mellitus: a clinical practice guideline from the American College of Physicians. *Ann.*

Intern. Med. 156:218–231. https://doi.org/10.7326/0003-4819-156-3 -201202070-00011

Schmid-Burgk, J.L., D. Chauhan, T. Schmidt, T.S. Ebert, J. Reinhardt, E. Endl, and V. Hornung. 2016. A genome-wide CRISPR (clustered regularly interspaced short palindromic repeats) screen identifies NEK7 as an essential component of NLRP3 inflammasome activation. *J. Biol. Chem.* 291:103–109. https://doi.org/10.1074/jbc.C115.700492

Shi, H., Y. Wang, X. Li, X. Zhan, M. Tang, M. Fina, L. Su, D. Pratt, C.H. Bu, S. Hildebrand, et al. 2016. NLRP3 activation and mitosis are mutually exclusive events coordinated by NEK7, a new inflammasome component. *Nat. Immunol.* 17:250–258. https://doi.org/10.1038/ni.3333

Snouwaert, J.N., K.K. Brigman, A.M. Latour, N.N. Malouf, R.C. Boucher, O. Smithies, and B.H. Koller. 1992. An animal model for cystic fibrosis made by gene targeting. *Science.* 257:1083–1088. https://doi.org/10 .1126/science.257.5073.1083

So, A., T. De Smedt, S. Revaz, and J. Tschopp. 2007. A pilot study of IL-1 inhibition by anakinra in acute gout. *Arthritis Res. Ther.* 9:R28. https:// doi.org/10.1186/ar2143

Sonawane, N.D., and A.S. Verkman. 2008. Thiazolidinone CFTR inhibitors with improved water solubility identified by structure-activity analysis. *Bioorg. Med. Chem.* 16:8187–8195. https://doi.org/10.1016/j.bmc.2008 .07.044

Stienstra, R., L.A. Joosten, T. Koenen, B. van Tits, J.A. van Diepen, S.A. van den Berg, P.C. Rensen, P.J. Voshol, G. Fantuzzi, A. Hijmans, et al. 2010. The inflammasome-mediated caspase-1 activation controls adipocyte differentiation and insulin sensitivity. *Cell Metab.* 12:593–605. https:// doi.org/10.1016/j.cmet.2010.11.011

Strickson, S., D.G. Campbell, C.H. Emmerich, A. Knebel, L. Plater, M.S. Ritorto, N. Shpiro, and P. Cohen. 2013. The anti-inflammatory drug BAY 11-7082 suppresses the MyD88-dependent signalling network by targeting the ubiquitin system. *Biochem. J.* 451:427–437. https://doi.org /10.1042/BJ20121651

Terkeltaub, R., J.S. Sundy, H.R. Schumacher, F. Murphy, S. Bookbinder, S. Biedermann, R. Wu, S. Mellis, and A. Radin. 2009. The interleukin 1 inhibitor rilonacept in treatment of chronic gouty arthritis: results of a placebo-controlled, monosequence crossover, non-randomised, single-blind pilot study. *Ann. Rheum. Dis.* 68:1613–1617. https://doi.org/10 .1136/ard.2009.108936

Ting, J.P., D.L. Kastner, and H.M. Hoffman. 2006. CATERPILLERs, pyrin and hereditary immunological disorders. *Nat. Rev. Immunol.* 6:183–195. https://doi.org/10.1038/nri1788

Wang, W.Y., Y.C. Wu, and C.C. Wu. 2006. Prevention of platelet glycoprotein IIb/IIIa activation by 3,4-methylenedioxy-beta-nitrostyrene, a novel tyrosine kinase inhibitor. *Mol. Pharmacol.* 70:1380–1389. https://doi.org /10.1124/mol.106.023986

Wen, H., D. Gris, Y. Lei, S. Jha, L. Zhang, M.T. Huang, W.J. Brickey, and J.P. Ting. 2011. Fatty acid-induced NLRP3-ASC inflammasome activation interferes with insulin signaling. *Nat. Immunol.* 12:408–415. https://doi .org/10.1038/ni.2022

Yan, Y., W. Jiang, T. Spinetti, A. Tardivel, R. Castillo, C. Bourquin, G. Guarda, Z. Tian, J. Tschopp, and R. Zhou. 2013. Omega-3 fatty acids prevent inflammation and metabolic disorder through inhibition of NLRP3 inflammasome activation. *Immunity.* 38:1154–1163. https://doi.org/10 .1016/j.immuni.2013.05.015

Yan, Y., W. Jiang, L. Liu, X. Wang, C. Ding, Z. Tian, and R. Zhou. 2015. Dopamine controls systemic inflammation through inhibition of NLRP3 inflammasome. *Cell.* 160:62–73. https://doi.org/10.1016/j.cell .2014.11.047

Yip, K.H., M.H. Zheng, H.T. Feng, J.H. Steer, D.A. Joyce, and J. Xu. 2004. Sesquiterpene lactone parthenolide blocks lipopolysaccharide-induced osteolysis through the suppression of NF-kappaB activity. *J. Bone Miner. Res.* 19:1905–1916. https://doi.org/10.1359/JBMR.040919

Youm, Y.H., K.Y. Nguyen, R.W. Grant, E.L. Goldberg, M. Bodogai, D. Kim, D. D'Agostino, N. Planavsky, C. Lupfer, T.D. Kanneganti, et al. 2015. The ketone metabolite β-hydroxybutyrate blocks NLRP3 inflammasome-mediated inflammatory disease. *Nat. Med.* 21:263–269. https://doi.org /10.1038/nm.3804

Zhou, R., A. Tardivel, B. Thorens, I. Choi, and J. Tschopp. 2010. Thioredoxin-interacting protein links oxidative stress to inflammasome activation. *Nat. Immunol.* 11:136–140. https://doi.org/10.1038/ni.1831

Zhou, R., A.S. Yazdi, P. Menu, and J. Tschopp. 2011. A role for mitochondria in NLRP3 inflammasome activation. *Nature.* 469:221–225. https://doi .org/10.1038/nature09663